Berger, W.H., Kroenke, L.W., Mayer, L.A., et al., 1993
Proceedings of the Ocean Drilling Program, Scientific Results, Vol. 130

29. FORAMINIFER PRESERVATION RECORD FOR THE LAST MILLION YEARS: SITE 805, ONTONG JAVA PLATEAU[1]

M. Yasuda,[2] W.H. Berger,[2] G. Wu,[2,4] S. Burke,[2] and H. Schmidt[3]

ABSTRACT

Downcore changes in various carbonate dissolution indexes are documented for Hole 805C for the last 1.2 m.y. These indexes include degree of fragmentation of planktonic foraminifers, percent sand, abundance ratio of species of contrasting solution susceptibilities (*Globigerinoides sacculifer* vs. *Pulleniatina, Globorotalia tumida,* and *Globorotalia menardii*), and the difference in $\delta^{18}O$ between species of contrasting solution susceptibilities (*G. sacculifer* vs. *Pulleniatina*). These preservation indexes have been combined into a single composite dissolution index that corresponds closely to the $\delta^{18}O$ record. The rate of change of the oxygen isotope signal is also important, with glacial-to-interglacial transitions corresponding to maximum preservation events and vice versa. For information on changing productivity (which is important because an increased supply of organic matter may enhance dissolution by lowering pH upon degradation), we present the abundance of coarse-fraction benthic foraminifers per gram and the ratio between two planktonic foraminiferal species, one of which is strongly associated with equatorial upwelling (*Globorotalia tumida* vs. *Pulleniatina*). Our results suggest that productivity plays a subordinate role in determining foraminifer preservation. Furthermore, our results confirm previous observations that associate enhanced preservation events with glacial periods and with glacial-to-interglacial transitions. A correlation between preservation and sedimentation rates of these carbonate-rich sediments could not be established. Notable differences are present between the responses of individual dissolution indexes, indicating that processes other than dissolution determine proxy indexes to varying degrees.

INTRODUCTION

The carbonate cycles in Quaternary deep-sea sediments of the equatorial Pacific were discovered some 40 yr ago during the Swedish Deep-Sea Expedition and stimulated thinking about cyclic changes in ocean productivity driven by glacial-interglacial changes in the intensity of upwelling (Arrhenius, 1952). The exact mode of origin of these carbonate cycles is still unknown even though much study since their discovery has produced detailed information on carbonate distributions and on stable isotope and preservation stratigraphies in both the eastern and western equatorial Pacific (Hays et al., 1969; Berger, 1973; Shackleton and Opdyke, 1973, 1976; Thompson and Saito, 1974; Luz and Shackleton, 1975; Pisias, 1976; Thompson, 1976; Moore et al., 1977, 1982; Valencia, 1977; Adelseck, 1977; Adelseck and Anderson, 1978; Volat et al., 1980; Gardner, 1982; Schiffelbein, 1984; Schiffelbein and Dorman, 1986; Crowley, 1985; Chuey et al., 1987; Lyle et al., 1988; Farrell and Prell, 1989, 1991; Wu and Berger, 1989, 1991; Hebbeln et al., 1990; Wu et al., 1990, 1991; Grötsch et al., 1991; Le and Shackleton, 1992).

Discussions have centered on quantifying the relative importance of fluctuations in supply vs. dissolution in determining percent carbonate because of interest in the marine carbon cycle. Much evidence exists that basin-wide dissolution cycles have produced correlatable carbonate cycles within a glacial/interglacial time frame (Berger and Vincent, 1981; Vincent, 1985). Equally strong evidence exists in favor of the productivity concept (Arrhenius, 1952, 1988). The question cannot be answered from a knowledge of carbonate cycles alone, if the limits allowed for productivity variations are suitably wide (Berger, 1992). Recent calculations by Archer (1991) suggest that a twofold increase in glacial production is sufficient to explain the variations in carbonate accumulation rates, although concurrent changes in Pacific deep-water carbonate saturation are not discounted by him. Archer's estimate of the range of glacial/interglacial productivity is within the range of variation found in the modern ocean, unlike some previous estimates. Herguera and Berger (1991) suggest factors of 1.6–2.0 for the glacial vs. postglacial productivity contrast on Ontong Java Plateau. To complicate matters, net carbonate accumulation is also affected by increased organic-matter supply, which is presumably positively correlated with increased carbonate supply. Oxidation of organic matter (C_{org}) should increase carbonate dissolution by lowering pH at and immediately below the seafloor. However, this dissolution mechanism may only be important if C_{org} is not oxidized before being incorporated into the mixed layer (Archer, 1991). Thus, this process may be of decreasing importance as depth to seafloor increases. Redeposition processes must also be considered. Differences in carbonate content between Leg 130 sites at different depths are insufficient to explain differences in sedimentation rates, if carbonate dissolution is assumed to be the cause of the depth gradient in sediment accumulation (Berger et al., 1991). Thus, the fate of noncarbonate dilutants or winnowing must be important and changes in the intensity of these factors must play a role in producing the cycles.

In the western equatorial Pacific, at depths above the lysocline, carbonate content is uniformly high (near 85%–90%) in the Quaternary, and fluctuations are low (typically, within a range of about 6%). Changes in the percentages of $CaCO_3$ are not a sensitive indicator of the history of carbonate dissolution at these high carbonate concentrations, even when complications introduced by fluctuations in dilution with noncarbonate material can be assumed to be at a minimum, as at this site. Therefore, we construct a stratigraphy of foraminifer preservation in the western equatorial Pacific. If the preservational signal may be interpreted in terms of saturation of deep waters, at least in large part (Berger, 1977; Berger and Keir, 1984), in principle it should be possible to reconstruct the fluctuations of deep-water saturation (Keir and Berger, 1983; Peterson and Prell, 1985a, 1985b; Hebbeln et al., 1990; Grötsch et al., 1991). We also construct a stratigraphy of productivity, based on the abundance of benthic foraminifers and changes in the composition of the pelagic assemblage, in order to estimate the importance of productivity to carbonate preservation.

[1] Berger, W.H., Kroenke, L.W., Mayer, L.A., et al., 1993. *Proc. ODP, Sci. Results,* 130: College Station, TX (Ocean Drilling Program).
[2] Geological Research Division, Scripps Institution of Oceanography, University of California, San Diego, La Jolla, CA 92093, U.S.A.
[3] Fachbereich Geowissenschaften, Universität Bremen, Postfach 330440, 2800 Bremen 33, Federal Republic of Germany.
[4] Present address: Université du Québec à Montréal, GEOTOP, Case postale 8888, succursale A, Montréal, Québec, H3C 3P8, Canada.

We report here on the upper 20 m recovered from Hole 805C, comprising Cores 130-805C-1H and -2H, and the upper portion of Core 130-805C-3H. Site 805 was drilled during Ocean Drilling Program (ODP) Leg 130, at 1°13.9′ N, 160°31.77′E, in 3188 m of water. This depth is just above the present regional lysocline (near 3.3 km; Wu and Berger, 1991). We also use data from Hole 806B for comparison (from Berger et al., this volume). Site 806 was drilled at 00°10.11′ N, 159°21.69′E, in 2520 m of water. The location of the two sites is shown in Figure 1.

MEASUREMENTS

Samples used in this study are from Hole 805C, from the sediment surface down through the upper portion of Core 130-805C-3H near 20 m, except for measurements involving planktonic foraminifer counts, which are from the sediment surface down through the bottom of Core 130-805C-2H near 17 m. The typical sample spacing is 10 cm. The Brunhes/Matuyama boundary was detected at 12.7 m (official ODP depth) within Core 130-805C-2H (Shipboard Scientific Party, 1991). Assuming an age of 790,000 yr for the Brunhes/Matuyama boundary (Shackleton et al., 1990; Izett and Obradovich, 1991), the average sedimentation rate above this boundary is near 1.6 cm/k.y. and the typical sampling interval represents 6000 yr. The age of the oldest sediment studied, at 20 m below seafloor (mbsf), is estimated to be near 1.2 m.y., based on linear extrapolation of the sedimentation rate above the Brunhes/Matuyama boundary.

Our measurements of dissolution characteristics include degree of planktonic foraminifer fragmentation; relative abundance of whole *Globigerinoides sacculifer* vs. the sum of whole *Globigerinoides sacculifer,* whole *Pulleniatina,* whole *Globorotalia tumida,* and whole *Globorotalia menardii;* and percent sand-size fragments (Table 1). In addition, the $\delta^{18}O$ record of planktonic foraminifers (Berger et al., this volume) is used to interpret the dissolution stratigraphy. Although benthic foraminifer abundance has been correlated with intensity of dissolution (Parker and Berger, 1971; Thunell, 1976), it is not used here as a preservation index because of the strong productivity signal carried by this variable (Herguera and Berger, 1991). As mentioned, percent carbonate is not a very sensitive measure of dissolution above the lysocline on Ontong Java Plateau; therefore, we do not use it as a dissolution index. Within our sampling interval, the percent carbonate fluctuates in a narrow range from 84% to 92% (Shipboard Scientific Party, 1991).

To check whether any substantial relationship exists between productivity and dissolution, we use two productivity proxies: the total abundance of benthic foraminifers and the relative abundance of whole *Globorotalia tumida* vs. the sum of whole *Pulleniatina* and whole *G. tumida.* These productivity indexes are nevertheless susceptible to dissolution effects. However, all species used in these productivity indexes are quite resistant to dissolution (Parker and Berger, 1971). Little preserved organic matter is present at our site. C_{org} values measured within the top meter of sediments at Ontong Java Plateau generally range between 0.1% and 0.3% (Price, 1988).

SAMPLE PREPARATION

For each sample, approximately 10 cm^3 of wet-bulk sediment were freeze dried and then weighed. All samples were disaggregated by soaking in a mixture of buffered CALGON solution and 5% hydrogen peroxide for approximately 1 hr. Samples were then wet sieved through a 63-μm mesh sieve for approximately 20 min, with an intervening 5-s ultrasonification to loosen small particles trapped inside individual tests. Samples were given a final 1-min rinse in deionized water. Samples were then dried overnight (or longer) at 55°C and then weighed to determine the weight percent of particles greater than sand size (>63 μm). Abundance of total benthic foraminifers was determined using the size fraction >250 μm. The fraction of planktonic foraminifer fragments and whole tests was determined in the size class 250–425 μm. The ratios of *G. sacculifer* vs. the sum of *G. sacculifer, Pulleniatina, G. menardii,* and *G. tumida*; and *G. tumida* vs. *Pulleniatina* plus *G. tumida* were determined using the size fraction 355–425 μm.

RESULTS

Preservation Indexes

Our measurements of indexes of preservation and productivity for Hole 805C are listed in Tables 1 and 2 according to official ODP depths. All raw data are available from the first author. Preservation indexes are plotted vs. corrected depth in Figure 2. Our preservation indexes in Figure 2 look quite similar at a glance, except for the difference in $\delta^{18}O$ between *G. sacculifer* and *Pulleniatina* (marked "POX-SOX" on the graph, data from Berger et al., this volume). The oxygen isotope record of *Pulleniatina* (POX) is given for guidance. The record of this species is somewhat less sensitive to the effects of differential dissolution than that of *G. sacculifer* (Wu and Berger, 1989).

A depth correction has been applied to all data displayed in the following graphs to avoid the apparent overlap of cores that occurs when using official ODP depth assignments. Depth corrections are necessitated because of the recovery of excess core (presumably from core expansion) and because of sampling gaps. Sampling gaps have been identified by comparison of matching physical properties between offset cores. Gaps between cores were estimated as 30 cm (Berger et al., this volume), based on comparisons of $\delta^{18}O$ records for Hole 805C with those of nearby Cores V28-238 and V28-239 and on visual comparisons of GRAPE data for offset Holes 805A, 805B, and 805C. After adding back the presumed length of missing core, excess core recovery was adjusted to fit within official ODP core length assignments based on the assumption that the official depths at the tops of all cores is correct. In summary, the official ODP core depths were corrected by applying the following factors: H1 = 0.9615 (ODP depth), H2 = 0.9312 (ODP depth), and H3 = 0.9787 (ODP depth). A more detailed description of the Hole 805C depth correction is given in Berger et al. (this volume).

For discussion in terms of age, we include an estimation of age vs. depth based on counting obliquity and eccentricity cycles. Our age assignments are listed in Table 3. The 100- and 41-k.y. wavelength components of the $\delta^{18}O$ *Pulleniatina* record were reconstructed by extracting the signal within a ±15% band of the expected harmonics containing these components. The reconstructed 100- and 41-k.y. signals are shown in Figure 3. By counting crests in the obliquity-related signal, we were able to assign depth increments to time increments of 41-k.y. Assignments of 41-k.y. spacing were based on best agreement with the spacing of the 100-k.y. cycles. The age of the isotopic stage 16/15 termination is near 623 k.y. in our scale (Fig. 3), in good agreement with the assignment of 618 k.y. of Imbrie et al. (1984). Below this level, our age assignments for the same isotopic features are older than theirs. The method used here for extraction of the obliquity and eccentricity components is identical to that described in detail by Berger et al. (this volume), except that our data was processed as a single continuous data set rather than as three shorter data sets (individual cores). Our age model is intended as a rough guide only. We did not adopt existing age models because of the controversy surrounding the true age of the Brunhes/Matuyama boundary (see Shackleton et al., 1990; Izett and Obradovich, 1991).

Fragmentation

For the fragmentation record (Berger, 1970a; Thompson, 1976; Thunell, 1976), we use the percent abundance of whole tests of all planktonic foraminifers and the percent abundance of whole tests within the *G. menardii* complex (*Globorotalia menardii* and *Globorotalia tumida*) (Table 1 and Fig. 2). Fragmentation of the *G. menardii* complex closely parallels the general fragmentation record,

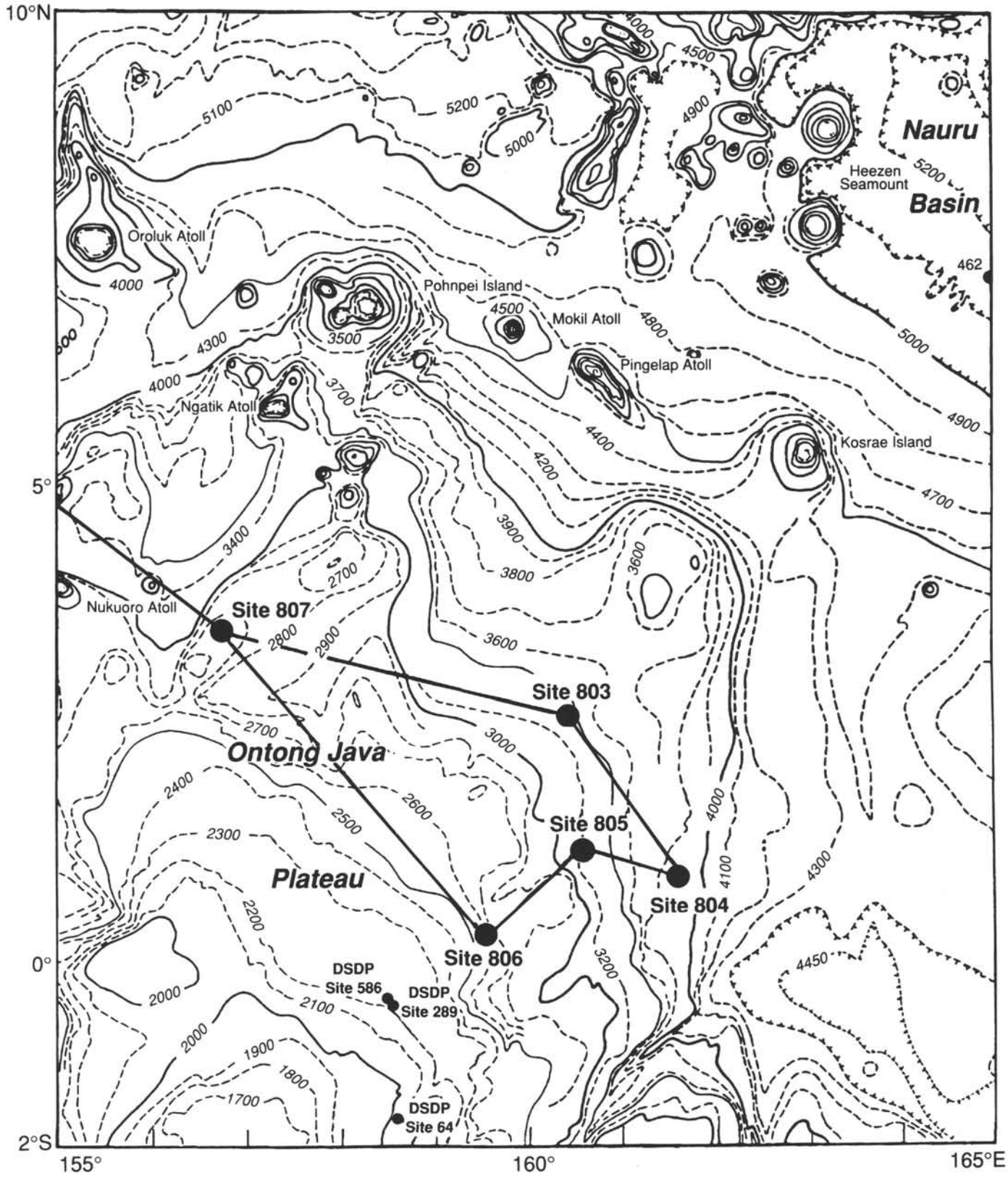

Figure 1. Location map.

Table 1. Preservation indexes, Hole 805C.

Core, section, interval (cm)	Depth* (mbsf)	% Sand fraction >63 µm (%)	Fragmentation		Planktonic Ratio [#SAC/ (#SAC+ #PUL+ #MENA+ #TUMI)]†
			Whole *G. menardii* (%)	Whole tests (%)	
1H-1, 9–11	0.09	25.18	20.2	42.9	
1H-1, 13–15	0.13	44.72	42.6	71.9	0.3
1H-1, 19–21	0.19	43.33	41.5	64.4	
1H-1, 19–21	0.19		42.1	60.6	
1H-1, 21–23	0.21	37.19	44.6	58.9	0.5
1H-1, 29–31	0.29	25.26	40.2	66.0	0.4
1H-1, 39–41	0.39	29.76	53.6	50.8	0.3
1H-1, 39–41	0.39				
1H-1, 49–51	0.49	33.15	47.8	51.1	0.3
1H-1, 59–61	0.59	27.51	54.6	56.5	0.2
1H-1, 69–71	0.69	24.95	34.0	47.4	0.2
1H-1, 69–71	0.69				0.2
1H-1, 75–77	0.75	27.55			
1H-1, 89–91	0.89	32.84	49.7	60.3	0.3
1H-1, 89–91	0.89				0.3
1H-1, 89–91	0.89				0.3
1H-1, 99–101	0.99	28.07	41.9	41.7	0.2
1H-1, 109–111	1.09	19.52	35.9	32.9	0.1
1H-1, 119–121	1.19	27.08	23.8	42.8	0.3
1H-1, 129–131	1.29	40.77	44.2	58.9	0.5
1H-1, 139–141	1.39	19.91			
1H-1, 143–145	1.43	22.04	20.4	25.6	0.1
1H-2, 4–6	1.54	31.93	40.4	46.3	0.4
1H-2, 19–21	1.69	18.63	22.9	20.9	0.1
1H-2, 29–31	1.79	38.20	81.5	77.7	0.5
1H-2, 39–41	1.89	40.73	63.0	69.0	0.4
1H-2, 49–51	1.99	27.56	59.1	67.3	0.4
1H-2, 49–51	1.99				0.4
1H-2, 59–61	2.09	37.62	60.0	70.0	0.6
1H-2, 69–71	2.19	37.88	54.5	62.4	0.6
1H-2, 79–81	2.29	25.80	53.2	60.3	0.5
1H-2, 89–91	2.39	39.32	32.0	46.4	0.4
1H-2, 99–101	2.49	29.17	45.2	46.2	0.4
1H-2, 109–111	2.59	25.14	57.2	48.8	0.4
1H-2, 119–121	2.69	15.65	30.6	47.6	0.3
1H-2, 129–131	2.79	16.42	17.0	47.8	0.2
1H-2, 143–145	2.93	12.18			
1H-2, 148–150	2.98	19.52	31.5	34.0	0.2
1H-3, 9–11	3.09	37.47	41.4	54.4	0.7
1H-3, 19–21	3.19	25.67	42.6	50.8	0.6
1H-3, 19–21	3.19				0.7
1H-3, 29–31	3.29	17.38	49.8	52.2	0.5
1H-3, 39–41	3.39	30.42	52.2	42.5	0.5
1H-3, 49–51	3.49	41.28	57.2	64.6	0.7
1H-3, 49–51	3.49		54.7	64.0	
1H-3, 59–61	3.59	35.58			
1H-3, 69–71	3.69	23.84	57.1	64.9	0.5
1H-3, 79–81	3.79	30.62	70.9	65.5	0.5
1H-3, 79–81	3.79		61.5	69.2	
1H-3, 89–91	3.89	27.20	63.0	58.2	0.5
1H-3, 99–101	3.99	13.67	60.5	31.7	0.3
1H-3, 99–101	3.99				0.3
1H-3, 109–111	4.09	12.48	66.9	39.8	0.5
1H-3, 119–121	4.19	22.02	56.8	42.0	0.4
1H-3, 129–131	4.29	13.41	62.4	36.5	0.2
1H-3, 139–141	4.39	11.45	74.8	27.5	0.2
1H-3, 148–150	4.48	11.13	46.2	21.4	0.2
1H-4, 11–13	4.61	12.85			
1H-4, 19–21	4.69	15.84	45.5	31.5	0.2
1H-4, 29–31	4.79	7.42	31.0	36.6	0.1
1H-4, 38–40	4.88	19.23			
1H-4, 49–51	4.99	23.54	55.3	53.0	0.6
1H-4, 59–61	5.09	28.95	57.0	58.8	0.6
1H-4, 69–71	5.19	22.92	51.5	52.7	0.5
1H-4, 89–91	5.39	24.27	42.9	53.0	0.4
1H-4, 89–91	5.39		38.7	46.0	
1H-4, 99–101	5.49	11.06	32.3	40.0	0.1
1H-4, 109–111	5.59	12.57	36.5	30.0	0.1
1H-5, 9–11	6.09	13.01	22.9	22.5	0.1
1H-5, 19–21	6.19	21.20	53.3	29.2	0.2
1H-5, 29–31	6.29	31.74	68.1	54.3	0.6
1H-5, 39–41	6.39	30.92	64.9	62.8	0.4
1H-5, 49–51	6.49	29.20	70.0	52.9	0.4
1H-5, 49–51	6.49				0.4
1H-5, 59–61	6.59	23.26	58.1	51.5	0.2
1H-5, 69–71	6.69	21.17	65.8	57.3	0.2
1H-5, 79–81	6.79	21.40	61.4	52.4	0.2
1H-5, 89–91	6.89	18.95	51.7	48.6	0.2
1H-5, 99–101	6.99	15.95	40.1	51.7	0.2
1H-5, 109–111	7.09	19.32	28.1	39.8	0.2
1H-5, 119–121	7.19	19.01	33.3	51.5	0.3
1H-5, 119–121	7.19				0.3
1H-5, 129–131	7.29	9.33	20.0	36.8	0.1
1H-5, 129–131	7.29		28.1	37.0	
1H-5, 142–145	7.42	9.58	14.9	17.1	0.1
1H-5, 149–151	7.49	12.10	25.9	25.1	0.1
2H-1, 9–11	7.95	18.63	47.0	52.3	0.1
2H-1, 19–21	7.99	16.41	39.9	52.3	0.2
2H-1, 29–31	8.09	14.88	43.5	38.7	0.2
2H-1, 39–41	8.19	7.88	29.8	41.6	0.1
2H-1, 49–51	8.29	12.53	29.2	40.8	0.1
2H-1, 49–51	8.29				0.0
2H-1, 59–61	8.39	18.27	32.2	33.3	0.2
2H-1, 69–71	8.49	16.38	43.1	50.4	0.2
2H-1, 79–81	8.59	21.69	51.6	59.3	0.3
2H-1, 89–91	8.69	11.61	41.9	48.9	0.1
2H-1, 99–101	8.79	13.38	43.9	48.8	0.2
2H-1, 109–111	8.89	11.89	43.5	45.6	0.1
2H-1, 119–121	8.99	15.50	36.3	50.8	0.1
2H-1, 129–131	9.09	15.99	50.3	54.7	0.1
2H-1, 139–141	9.19	12.12	25.9	45.2	0.2
2H-1, 139–141	9.19				0.1
2H-1, 148–150	9.28	20.34	48.6	51.4	0.3
2H-2, 9–11	9.39	17.69	54.3	53.5	0.3
2H-2, 19–21	9.49	16.68	48.7	58.9	0.2
2H-2, 29–31	9.59	28.21	65.6	81.4	0.5
2H-2, 39–41	9.69	31.09	73.4	77.7	0.4
2H-2, 49–51	9.79	33.19	64.6	71.1	0.4
2H-2, 59–61	9.89	29.91	76.8	76.2	0.3
2H-2, 69–71	9.99	30.24	76.3	77.9	0.4
2H-2, 79–81	10.09	28.69	65.9	72.5	0.4
2H-2, 89–91	10.19	30.70	66.7	70.4	0.3
2H-2, 99–101	10.29	28.83	69.6	74.4	0.3
2H-2, 109–111	10.39	33.71	63.3	76.8	0.3
2H-2, 109–111	10.39		69.3	77.5	
2H-2, 119–121	10.49	28.44	80.4	78.1	0.3
2H-2, 129–131	10.59	30.12	61.5	75.7	0.3
2H-2, 139–141	10.69	25.85	53.5	71.1	0.3
2H-2, 148–150	10.78	26.38	68.6	76.2	0.3
2H-3, 9–11	10.89	20.75	64.7	68.3	0.3
2H-3, 19–21	10.99	22.76	71.3	74.5	0.3
2H-3, 20–22	11.00	21.79			
2H-3, 29–31	11.09	15.32	42.7	61.6	0.2
2H-3, 29–31	11.09		42.7		0.2
2H-3, 39–41	11.19	9.63	20.8	38.6	0.1
2H-3, 49–51	11.29	23.61	43.9	35.2	0.4
2H-3, 59–61	11.39	24.86	60.3	68.5	0.4
2H-3, 69–71	11.49	25.72	60.0	63.0	0.4
2H-3, 79–81	11.59	22.47	44.0	64.4	0.3
2H-3, 89–91	11.69	19.07	32.2	53.2	0.2
2H-3, 99–101	11.79	23.72	54.3	60.3	0.3
2H-3, 109–111	11.89	30.22	60.1	74.0	0.4
2H-3, 119–121	11.99	31.20	66.5	72.0	0.3
2H-3, 129–131	12.09	13.57	51.2	44.6	0.2
2H-3, 139–141	12.19	15.81	48.0	48.4	0.2
2H-3, 148–150	12.28	11.72	39.4	46.5	0.2
2H-4, 9–11	12.39	10.99	23.2	45.0	0.1
2H-4, 19–21	12.49	15.18	37.7	52.2	0.3
2H-4, 29–31	12.59	12.57	24.3	36.7	0.1
2H-4, 39–41	12.69	27.38	54.4	50.4	0.5
2H-4, 39–41	12.69		54.4		0.5
2H-4, 49–51	12.79	27.84	52.5	64.1	0.5
2H-4, 59–61	12.89	16.59	59.1	62.2	0.4
2H-4, 69–71	12.99	18.88	55.2	55.5	0.2

Table 1 (continued).

Core, section, interval (cm)	Depth* (mbsf)	% Sand fraction >63 µm (%)	Fragmentation		Planktonic Ratio [#SAC/ (#SAC+ #PUL+ #MENA+ #TUMI)]†
			Whole *G. menardii* (%)	Whole tests (%)	
2H-4, 79–81	13.09	19.80	43.9	48.2	0.3
2H-4, 89–91	13.19	15.86	46.5	57.3	0.4
2H-4, 99–101	13.29	14.33	35.1	47.2	0.1
2H-4, 109–111	13.39	18.57	36.5	39.7	0.2
2H-4, 119–121	13.49	18.49	30.7	51.7	0.2
2H-4, 129–131	13.59	17.79	38.9	50.4	0.2
2H-4, 139–141	13.69	11.53	25.6	36.3	0.1
2H-4, 139–141	13.69		21.8	36.5	
2H-5, 9–11	13.89	10.99	32.3	41.4	0.1
2H-5, 19–21	13.99	17.22	30.9	36.7	0.2
2H-5, 29–31	14.09	23.93	59.6	64.8	0.4
2H-5, 39–41	14.19	27.90	67.1	69.5	0.5
2H-5, 49–51	14.29	24.34	62.2	64.7	0.4
2H-5, 59–61	14.39	26.88	55.8	67.5	0.3
2H-5, 69–71	14.49	28.76	72.4	71.8	0.3
2H-5, 69–71	14.49		67.0	67.7	
2H-5, 79–81	14.59	19.40	44.9	49.4	0.3
2H-5, 89–91	14.69	18.13	55.9	56.5	0.3
2H-5, 99–101	14.79	24.38	56.8	70.1	0.3
2H-5, 109–111	14.89	28.31	56.5	70.1	0.3
2H-5, 119–121	14.99	31.62	49.2	69.2	0.3
2H-5, 129–131	15.09	16.19	59.7	60.8	0.2
2H-5, 139–141	15.19	19.17	43.2	42.0	0.1
2H-6, 9–11	15.39	3.63	34.9	31.3	0.1
2H-6, 12–14	15.42	8.98			
2H-6, 19–21	15.49	8.63	38.7	51.8	0.2
2H-6, 21–23	15.51	7.72			
2H-6, 32–34	15.62	7.75	21.8	33.3	0.0
2H-6, 39–41	15.69	10.38	26.0	29.4	0.0
2H-6, 49–51	15.79	12.06	62.9	60.7	0.1
2H-6, 59–61	15.89	14.37	44.7	58.8	0.4
2H-6, 69–71	15.99	16.69	26.1	56.7	0.6
2H-6, 79–81	16.09	14.29	36.2	58.3	0.4
2H-6, 89–91	16.19	5.31	41.2	51.3	0.0
2H-6, 99–101	16.29	7.31	40.7	41.6	0.1
2H-6, 102–104	16.32	7.01			
2H-6, 109–111	16.39	6.62	28.6	34.1	0.0
2H-6, 119–121	16.49	8.21	30.2	51.3	0.0
2H-6, 129–131	16.59	13.54	28.1	52.8	0.1
2H-6, 139–141	16.69	6.88	31.2	30.3	0.0
2H-6, 148–150	16.78	5.94	30.5	49.3	0.0
2H-7, 9–11	16.89	5.89	25.0	40.1	0.0
2H-7, 19–21	16.99	9.56	32.9	42.2	0.1
2H-7, 32–34	17.12	24.39	41.1	59.3	0.2
2H-7, 39–41	17.19	23.70	42.4	61.0	0.2
2H-7, 39–41	17.19				0.2
2H-7, 49–51	17.29	13.37	39.5	42.6	0.1
2H-7, 53–55	17.33	17.39			
2H-7, 59–61	17.39	12.47	35.0	47.0	0.1
2H-7, 69–71	17.49	17.10	25.6	49.2	0.1
3H-1, 9–11	17.39	19.37	48.5	54.6	
3H-1, 19–21	17.49	17.37	40.2	52.8	
3H-1, 29–31	17.59	16.16	42.9	49.8	
3H-1, 39–41	17.69	22.05	43.3	56.3	
3H-1, 49–51	17.79	30.41	66.5	71.5	
3H-1, 59–61	17.89	25.15	47.4	53.8	
3H-1, 69–71	17.99	18.22	24.7	34.2	
3H-1, 79–81	18.09	29.15	48.2	61.5	
3H-1, 89–91	18.19	33.36	37.3	56.3	
3H-1, 99–101	18.29	37.62			
3H-1, 109–111	18.39	39.95	69.6	75.1	
3H-1, 119–121	18.49	28.67			
3H-1, 129–131	18.59	26.31	72.2	73.5	
3H-1, 139–141	18.69	21.44	53.1	62.3	
3H-2, 9–11	18.89	18.58	26.3	30.4	
3H-2, 19–21	18.99	23.99	37.6	46.8	
3H-2, 24–26	19.04	24.97			
3H-2, 39–41	19.19	36.63	59.0	59.7	
3H-2, 49–51	19.29	33.91	58.1	71.3	
3H-2, 59–61	19.39	30.35	62.1	72.7	
3H-2, 69–71	19.49	19.95	44.0	50.2	
3H-2, 79–81	19.59	12.35	24.4	45.7	
3H-2, 89–91	19.69	13.17	22.8	36.2	
3H-2, 99–101	19.79	22.39	45.5	45.4	
3H-2, 109–111	19.89	34.61			
3H-2, 119–121	19.99	31.76	59.9	78.8	
3H-2, 129–131	20.09	20.82			
3H-2, 139–141	20.19	19.82	23.7	49.5	
3H-2, 148–150	20.28	15.68	27.6	41.3	

*ODP depth assignment = depth has not been adjusted.
†#SAC = the number of whole tests of *Globigerinoides sacculifer,* #PUL = the number of whole tests of *Pulleniatina,* #MENA = the number of whole tests of *Globorotalia menardii,* #TUMI = the number of whole tests of *Globorotalia tumida.*

indicating that differences in response between species are not great. In what follows, we have combined these two indexes, giving whole tests (WT) twice the weight of whole *G. menardii* (Wmen), because the WT is statistically more significant by virtue of its greater sample population than Wmen. The resulting composite fragmentation index (CFI) is defined as follows:

$$\mathrm{CFI} = \{(2[\mathrm{WT}] + [\mathrm{Wmen}])/3\}, \quad (1)$$

where square brackets denote variables in standard units (i.e., demeaned and divided by four times the standard deviation). The relationship between this index of fragmentation and the $\delta^{18}O$ record of *Pulleniatina* (POX) is presented in Figure 4. CFI is positive when fragmentation is low. POX is plotted positive up to demonstrate the correspondence with the fragmentation record. As expected from previous work, glacial periods (labeled with even isotopic stage numbers) correlate with increased abundance of whole tests. Upon closer inspection, one can also see that the preservation record "lags" the isotope record (as noted by Moore et al., 1977) because preservation peaks occur at the end of the glacial intervals. This shift can be explained if it is assumed that deglaciation leads to a decrease in carbonate dissolution on the seafloor, and vice versa (Shackleton, 1977; Berger and Vincent, 1981). A decrease in productivity during deglaciation (e.g., Herguera and Berger, 1991) can produce such an effect (Keir and Berger, 1983).

To visualize the phase relationship between CFI and the change in the $\delta^{18}O$ record, we compare CFI with a measure of the slope of the $\delta^{18}O$ *Pulleniatina* (POX′) record (Fig. 5). The derivative shown is one half of the $\delta^{18}O$ difference between points 20 cm apart, calculated at an incremental spacing of 10 cm. This simple method reduces the influence of spurious single points on the slope of the curve. The prominence of deglaciation events (labeled with the number of the preceding glaciation) is striking in this plot, supporting the asymmetric "saw-tooth" image of Broecker and van Donk (1970). There is a tendency for preservation peaks to approach the deglaciation peaks from below the level of maximum $\delta^{18}O$ change. However, aside from this tendency for coincidence of peak values, some mismatches occur in the two curves. To optimize the fit between the preservation index and the two $\delta^{18}O$ records (zero order and first derivative), we write an equation of the form:

$$\mathrm{CFI}_{\mathrm{est}} = \{(k_1[\mathrm{POX}]) + (k_2[\mathrm{POX}'])\}, \quad (2)$$

Table 2. Productivity indexes, Hole 805C.

Core, section, interval (cm)	Depth* (mbsf)	Planktonic ratio [#TUM/ (#PUL + #TUM)]†	Total benthic foraminifers (#/gm)	Core, section, interval (cm)	Depth* (mbsf)	Planktonic ratio [#TUM/ (#PUL + #TUM)]†	Total benthic foraminifers (#/gm)
1H-1, 9–11	0.09		32.5	1H-5, 142–145	7.42	0.8	13.2
1H-1, 13–15	0.13	0.9	18.9	1H-5, 149–151	7.49	0.7	14.7
1H-1, 19–21	0.19		25.7	2H-1, 9–11	7.89	0.7	19.4
1H-1, 21–23	0.21	0.9	25.8	2H-1, 19–21	7.99	0.7	27.0
1H-1, 29–31	0.29	0.8	27.1	2H-1, 29–31	8.09	0.7	23.5
1H-1, 39–41	0.39	0.9	24.6	2H-1, 39–41	8.19	0.6	23.1
1H-1, 49–51	0.49	0.8	39.3	2H-1, 49–51	8.29	0.8	21.1
1H-1, 59–61	0.59	0.9	22.7	2H-1, 49–51	8.29	0.7	
1H-1, 69–71	0.69	0.9	41.1	2H-1, 59–61	8.39	0.8	20.3
1H-1, 69–71	0.69	0.9		2H-1, 69–71	8.49	0.9	13.5
1H-1, 75–77	0.75		34.8	2H-1, 79–81	8.59	0.8	20.8
1H-1, 89–91	0.89	0.9	36.3	2H-1, 89–91	8.69	0.7	19.3
1H-1, 89–91	0.89	0.9		2H-1, 99–101	8.79	0.7	33.8
1H-1, 89–91	0.89	0.9		2H-1, 109–111	8.89	0.7	37.2
1H-1, 99–101	0.99	0.8	56.8	2H-1, 119–121	8.99	0.7	38.8
1H-1, 109–111	1.09	0.8	53.9	2H-1, 129–131	9.09	0.8	37.5
1H-1, 119–121	1.19	0.8	28.0	2H-1, 139–141	9.19	0.8	20.6
1H-1, 129–131	1.29	1.0	15.5	2H-1, 139–141	9.19	0.8	
1H-1, 143–145	1.43	0.8	31.4	2H-1, 148–150	9.28	0.8	19.7
1H-2, 4–6	1.54	0.6	23.8	2H-2, 9–11	9.39	0.8	15.3
1H-2, 19–21	1.69	0.8	31.1	2H-2, 19–21	9.49	0.8	16.2
1H-2, 29–31	1.79	0.9	20.5	2H-2, 29–31	9.59	0.7	29.0
1H-2, 39–41	1.89	0.6	39.5	2H-2, 39–41	9.69	0.7	38.0
1H-2, 49–51	1.99	0.8	38.4	2H-2, 49–51	9.79	0.7	36.9
1H-2, 59–61	2.09	0.8	46.6	2H-2, 59–61	9.89	0.7	32.3
1H-2, 69–71	2.19	0.8	46.0	2H-2, 69–71	9.99	0.8	35.0
1H-2, 79–81	2.29	0.8	61.1	2H-2, 79–81	10.09	0.8	29.7
1H-2, 89–91	2.39	0.8	85.7	2H-2, 89–91	10.19	0.8	35.3
1H-2, 99–101	2.49	0.8	55.9	2H-2, 99–101	10.29	0.8	34.6
1H-2, 109–111	2.59	0.8	51.9	2H-2, 109–111	10.39	0.8	40.3
1H-2, 119–121	2.69	0.8	70.0	2H-2, 119–121	10.49	0.8	36.3
1H-2, 129–131	2.79	0.8	64.2	2H-2, 129–131	10.59	0.7	36.4
1H-2, 143–145	2.93		14.5	2H-2, 139–141	10.69	0.7	36.2
1H-2, 148–150	2.98	0.7	19.1	2H-2, 148–150	10.78	0.7	43.8
1H-3, 9–11	3.09	0.9	19.7	2H-3, 9–11	10.89	0.7	34.6
1H-3, 19–21	3.19	0.8	21.1	2H-3, 19–21	10.99	0.8	
1H-3, 29–31	3.29	0.8	29.8	2H-3, 20–22	11.00		43.4
1H-3, 39–41	3.39	0.9	21.2	2H-3, 29–31	11.09	0.7	32.0
1H-3, 49–51	3.49	0.9	23.1	2H-3, 29–31	11.09	0.7	
1H-3, 59–61	3.59		36.5	2H-3, 39–41	11.19	0.7	21.7
1H-3, 69–71	3.69	0.8	40.3	2H-3, 49–51	11.29	0.8	18.8
1H-3, 79–81	3.79	0.8	37.4	2H-3, 59–61	11.39	0.8	7.0
1H-3, 89–91	3.89	0.7	41.2	2H-3, 69–71	11.49	0.8	22.6
1H-3, 99–101	3.99	0.7	46.7	2H-3, 79–81	11.59	0.8	29.2
1H-3, 99–101	3.99	0.7		2H-3, 89–91	11.69	0.7	39.5
1H-3, 109–111	4.09	0.8	42.4	2H-3, 99–101	11.79	0.8	28.0
1H-3, 119–121	4.19	0.9	17.0	2H-3, 109–111	11.89	0.9	
1H-3, 129–131	4.29	0.7	24.3	2H-3, 119–121	11.99	0.8	27.3
1H-3, 139–141	4.39	0.8	30.0	2H-3, 129–131	12.09	0.8	25.4
1H-3, 148–150	4.48	0.8	21.6	2H-3, 139–141	12.19	0.8	36.7
1H-4, 11–13	4.61		18.3	2H-3, 148–150	12.28	0.7	17.9
1H-4, 19–21	4.69	0.8	17.6	2H-4, 9–11	12.39	0.6	25.7
1H-4, 29–31	4.79	0.8	16.1	2H-4, 19–21	12.49	0.7	20.3
1H-4, 38–40	4.88		20.7	2H-4, 29–31	12.59	0.7	18.5
1H-4, 49–51	4.99	0.9		2H-4, 39–41	12.69	0.8	14.7
1H-4, 59–61	5.09	0.9	22.5	2H-4, 39–41	12.69	0.7	
1H-4, 69–71	5.19	0.8	37.1	2H-4, 49–51	12.79	0.8	18.1
1H-4, 89–91	5.39	0.6	27.2	2H-4, 59–61	12.89	0.8	19.1
1H-4, 99–101	5.49	0.6	29.4	2H-4, 69–71	12.99	0.7	42.4
1H-4, 109–111	5.59	0.6	33.9	2H-4, 79–81	13.09	0.6	56.2
1H-5, 9–11	6.09	0.9	9.9	2H-4, 89–91	13.19	0.7	30.2
1H-5, 19–21	6.19	0.9	12.3	2H-4, 99–101	13.29	0.8	32.9
1H-5, 29–31	6.29	0.9	15.3	2H-4, 109–111	13.39	0.9	18.0
1H-5, 39–41	6.39	0.8	11.6	2H-4, 119–121	13.49	0.9	26.0
1H-5, 49–51	6.49	0.8	21.2	2H-4, 129–131	13.59	0.8	19.3
1H-5, 49–51	6.49	0.7		2H-4, 139–141	13.69	0.8	20.3
1H-5, 59–61	6.59	0.7	37.3	2H-5, 9–11	13.89	0.8	15.3
1H-5, 69–71	6.69	0.6	31.6	2H-5, 19–21	13.99	0.9	18.1
1H-5, 79–81	6.79	0.8	28.9	2H-5, 29–31	14.09	0.9	14.6
1H-5, 89–91	6.89	0.7	25.2	2H-5, 39–41	14.19	0.7	30.5
1H-5, 99–101	6.99	0.8	22.6	2H-5, 49–51	14.29	0.7	36.9
1H-5, 109–111	7.09	0.7	32.3	2H-5, 59–61	14.39	0.6	28.4
1H-5, 119–121	7.19	0.8	23.1	2H-5, 69–71	14.49	0.7	35.2
1H-5, 129–131	7.29	0.7	24.3	2H-5, 79–81	14.59	0.8	36.7

Table 2 (continued).

Core, section, interval (cm)	Depth* (mbsf)	Planktonic ratio [#TUM/ (#PUL + #TUM)]†	Total benthic foraminifers (#/gm)	Core, section, interval (cm)	Depth* (mbsf)	Planktonic ratio [#TUM/ (#PUL + #TUM)]†	Total benthic foraminifers (#/gm)
2H-5, 89–91	14.69	0.8	35.0	2H-7, 69–71	17.49	0.5	60.3
2H-5, 99–101	14.79	0.8	23.6	3H-1, 9–11	17.39		18.0
2H-5, 109–111	14.89	0.9	23.3	3H-1, 19–21	17.49		37.7
2H-5, 119–121	14.99	0.9	29.9	3H-1, 29–31	17.59		29.1
2H-5, 129–131	15.09	0.9	36.8	3H-1, 39–41	17.69		42.8
2H-5, 139–141	15.19	0.8	57.2	3H-1, 49–51	17.79		34.9
2H-6, 9–11	15.39	0.4		3H-1, 59–61	17.89		41.3
2H-6, 12–14	15.42		48.1	3H-1, 69–71	17.99		23.2
2H-6, 19–21	15.49	0.5		3H-1, 79–81	18.09		15.2
2H-6, 21–23	15.51		28.7	3H-1, 89–91	18.19		24.8
2H-6, 32–34	15.62	0.6	18.9	3H-1, 99–101	18.29		27.5
2H-6, 39–41	15.69	0.7	22.7	3H-1, 109–111	18.39		26.0
2H-6, 49–51	15.79	0.9	13.1	3H-1, 119–121	18.49		28.2
2H-6, 59–61	15.89	0.9	13.7	3H-1, 129–131	18.59		30.2
2H-6, 69–71	15.99	0.8	20.1	3H-1, 139–141	18.69		29.1
2H-6, 79–81	16.09	0.8	31.1	3H-2, 9–11	18.89		33.9
2H-6, 89–91	16.19	0.6	36.6	3H-2, 19–21	18.99		28.4
2H-6, 99–101	16.29	0.5		3H-2, 24–26	19.04		33.2
2H-6, 109–111	16.39	0.5	42.1	3H-2, 39–41	19.19		24.1
2H-6, 119–121	16.49	0.7	31.8	3H-2, 49–51	19.29		30.9
2H-6, 129–131	16.59	0.8	22.6	3H-2, 59–61	19.39		51.6
2H-6, 139–141	16.69	0.8	22.6	3H-2, 69–71	19.49		54.1
2H-6, 148–150	16.78	0.6	26.6	3H-2, 79–81	19.59		25.6
2H-7, 9–11	16.89	0.5	30.6	3H-2, 89–91	19.69		
2H-7, 19–21	16.99	0.7	15.1	3H-2, 99–101	19.79		27.7
2H-7, 32–34	17.12	0.8	23.1	3H-2, 109–111	19.89		
2H-7, 39–41	17.19	0.8	28.0	3H-2, 119–121	19.99		35.5
2H-7, 39–41	17.19	0.8		3H-2, 129–131	20.09		32.4
2H-7, 49–51	17.29	0.7		3H-2, 139–141	20.19		43.7
2H-7, 53–55	17.33		85.2	3H-2, 148–150	20.28		52.2
2H-7, 59–61	17.39	0.4	48.5				

*ODP depth assignment = depth has not been adjusted.
†#TUM = the number of whole tests of *Globorotalia tumida,* and #PUL = the number of whole tests of *Pulleniatina.*

where the variables are as described and square brackets denote standardization. Requiring that the sum of squares of differences is minimized, and that the two coefficients add to unity, we obtain $k_1 = 0.6$ and $k_2 = 0.4$.

One can see that the CFI_{est} resulting from Equation (2) fits the original curve quite well over most of the record (Fig. 6), demonstrating that both the state of the ocean climate and its rate of change are important for the preservation of carbonate on the deep-sea floor. We also see from this exercise that preservation is particularly poor in the vicinity of Isotope Stage 13 (ca. 450–500 k.y. ago) and is particularly good for Stage 16 (ca. 600–650 ka), if we assume that preservation changes are driven by changes in [POX] and [POX′]. Furthermore, fluctuations in preservation are rather large in the lower portion of the record below 17 mbsf, where obliquity cycles dominate. These changes in the quality of the match suggest that the sensitivity of the preservation record to climatic forcing changes through time.

Sand Content

The sand content of deep-sea carbonates decreases as dissolution progresses on the Ontong Java Plateau (Johnson et al., 1977; Wu et al., 1991) and elsewhere. The reason is that the shells of foraminifers are weakened by partial dissolution and disintegrate both on the seafloor and during sample preparation. Thus, material moves from the coarse fraction into the finer fractions. Inspection of the fine sand in samples taken from greater depths on the seafloor, for example, reveals the presence of an increasing amount of small fragments originally belonging to larger shells. If this process is dominant, the whole-test index (CFI) should show good agreement with the percent sand record (SAND index). This is indeed the case over most of the record (Fig. 7). The correspondence is good to excellent for the time before Isotope Stage 8 (ca. 250 k.y.). In the uppermost portion, however, the sand content is much higher than expected from the abundance of whole tests. Thus, preservational effects alone cannot explain most of the sand record in the last 250 k.y. Other mechanisms producing variations, such as large changes in winnowing or bioturbation, must be invoked. It is not clear why the last 250 k.y. should be so different from the previous million years on this account. Apparently, winnowing activities greatly increased in this region in the latest Quaternary. If this change in dynamics is a general phenomenon, the common practice of using the history of the last 150 k.y. as a model for the previous million years must be viewed with caution.

Abundance of G. sacculifer

Tests of the species *G. sacculifer* are generally more susceptible to the effects of dissolution than the less porous tests of *Pulleniatina, G. menardii,* or *G. tumida.* All of these taxa are abundant in the western equatorial Pacific, so that their relative abundance is readily determined. Although this ratio may be influenced by climatic factors as well as preservational ones, Site 805 is deep enough that dissolution might be expected to deliver a strong overprint over the original ratios in the supply. The index we use (SAC index) is the percentage of whole *G. sacculifer* divided by the sum of whole *G. sacculifer,* whole *Pulleniatina,* whole *G. menardii,* and whole *G. tumida* (to dampen the effect of outliers in the ratio). Our count, as mentioned, only involves the upper two cores (Cores 130-805C-1H and -2H) to a depth of 17 mbsf (corrected). The correspondence of the SAC index with the CFI is quite good (Fig. 8) and bears out the expectation based on earlier work (Parker and Berger, 1971). Significant mismatches occur at Isotope Stages 8, 10, and 20 (*G. sacculifer* being much more

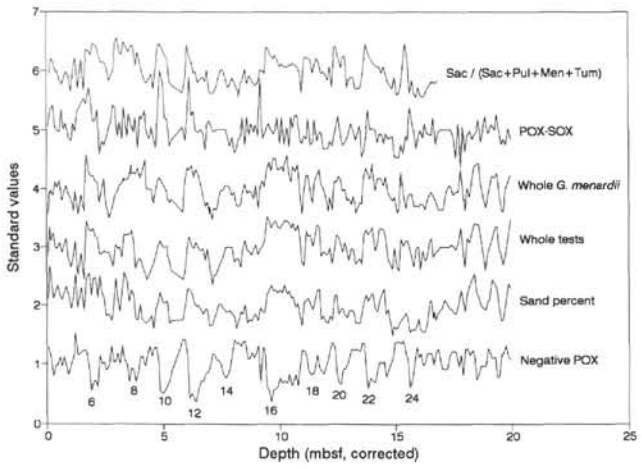

Figure 2. Preservation indexes and $\delta^{18}O$ for Hole 805C vs. corrected depth. The $\delta^{18}O$ record is given for reference. All fields in this figure and following figures are standardized according to (x-AVG)/[(4)(STD)]. Positive values indicate good preservation. Fields from the bottom up are negative $\delta^{18}O$ (*Pulleniatina*); sand fraction (wt% >63 mm); percent abundance of all whole planktonic foraminiferal tests relative to total number of particles in size fraction 250–425 µm; percent abundance of whole tests *G. menardii* complex relative to total number of particles in size fraction 250–425 µm; Δ $\delta^{18}O$ (*Pulleniatina* minus *G. sacculifer*); and number of tests of [(*G. sacculifer*)/(*G. sacculifer* + *Pulleniatina* + *G. menardii* + *G. tumida*)]. Isotopic stage numbers are given for reference in this figure and following figures.

abundant relative to *Pulleniatina, G. menardii,* and *G. tumida* than expected) and at Stage 16 (showing lower than expected abundance of *G. sacculifer*).

Summary

We have shown that the various preservation indexes (whole tests of foraminifers, sand content, and species abundance) correlate in the expected fashion, although mismatches and discrepancies exist in places. Generally, glacial intervals, as identified by the $\delta^{18}O$ record,

Table 3. Age-depth conversion based on 41-k.y. $\delta^{18}O$ obliquity cycle, Hole 805C.

Adjusted depth (m)	Age[a] (k.y.)	Age[b] (k.y.)	ΔAge[a,b] (k.y.)
0	0	0	0
1	65	72	–7
2	137	148	–11
3	204	225	–21
4	281	285	–4
5	346	351	–5
6	411	414	–3
7	474	477	–3
8	527	534	–7
9	590	593	–3
10	663	655	8
11	733	704	29
12	799	754	45
13	861	818	43
14	920	881	39
15	969	931	38
16	1026	983	43
17	1078	1039	39
18	1131	1091	40
19	1185	1144	41

[a] This study (*Pulleniatina*).
[b] Berger et al. (this volume, *G. sacculifer* and *Pulleniatina*).

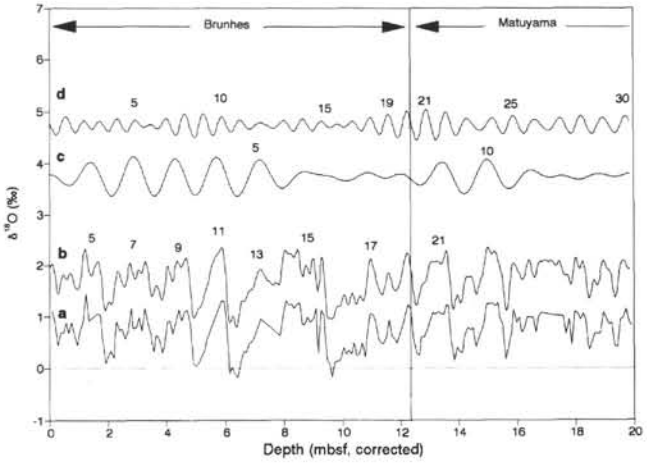

Figure 3. Obliquity and eccentricity components of Hole 805C $\delta^{18}O$ signal *Pulleniatina*; and $\delta^{18}O$ *Pulleniatina* vs. corrected depth. Fields from the bottom up are (a) negative $\delta^{18}O$ *Pulleniatina*; (b) reconstructed negative $\delta^{18}O$ using harmonics 1–80 (vertical offset: +1); (c) 100-k.y. eccentricity component using harmonics 10–15 (vertical offset: +3); and (d) 41-k.y. obliquity component using harmonics 25–35 (vertical offset: +4).

are characterized by good preservation, whereas the reverse is true for interglacials. In addition, the rate of change and its direction are important: deglaciation is associated with enhanced preservation, reglaciation is associated with increased dissolution. Combining all of these indexes into one,

$$CDI = \{0.5\ [CFI] + 0.25\ [SAND] + 0.25\ [SAC]\}, \quad (3)$$

yields a composite dissolution index (CDI) that corresponds very well with the $\delta^{18}O$ record (Fig. 9). In the fashion described in Equation (2), the best fit of CDI_{est} is obtained by setting the coefficients k_1 and k_2 to 0.55 and 0.45, respectively,

$$CDI_{est} = \{(k_1[POX]) + (k_2[POX'])\}, \quad (4)$$

indicating that the *state* of the system is roughly equal in importance to the *rate of change*. Additional information is necessary to determine

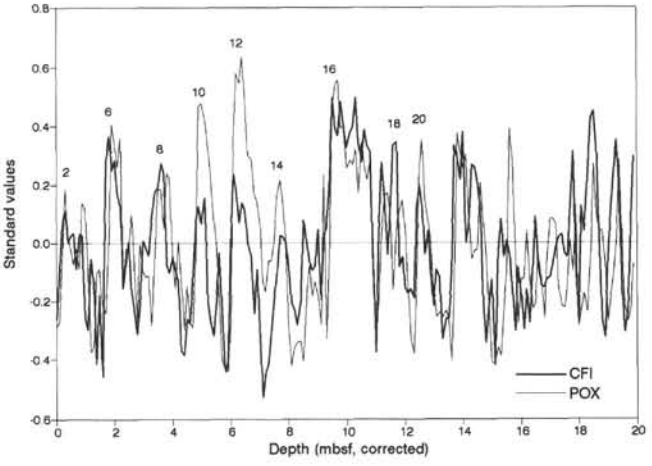

Figure 4. Standardized composite fragmentation index (CFI) and $\delta^{18}O$ *Pulleniatina* (POX) vs. corrected depth. CFI = (0.66) (standardized whole test index) + (0.33) (standardized *G. menardii* index). Positive CFI values indicate good preservation.

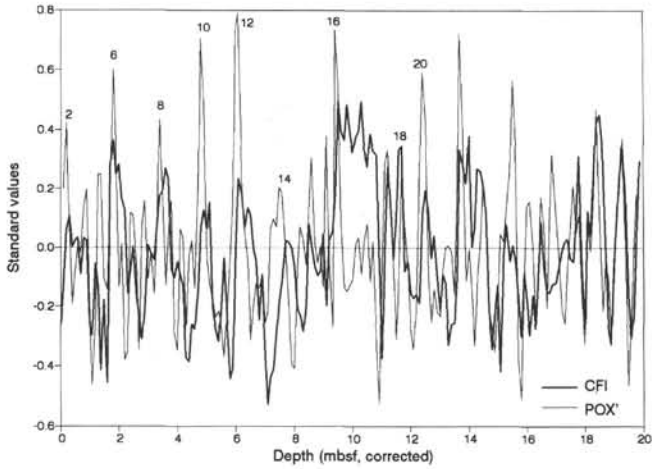

Figure 5. Standardized local change of $\delta^{18}O$ *Pulleniatina* (POX′) and CFI vs. corrected depth. The local change of $\delta^{18}O$ is one half of the difference between $\delta^{18}O$ values spaced 20 cm apart calculated at a 10-cm spacing. Evenly spaced data points were produced by interpolation. In essence, this is a quick approximation of the first derivative of the $\delta^{18}O$ curve, which reduces the effect of spurious single values. Positive CFI values indicate good preservation.

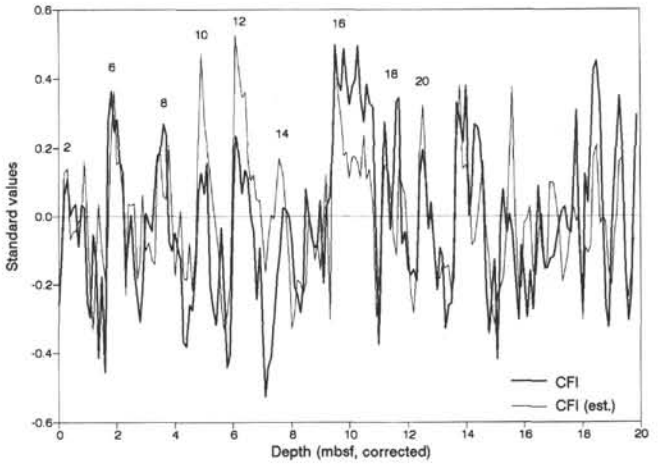

Figure 6. Standardized CFI (estimated) and standardized CFI vs. corrected depth. CFI (est.) = (0.6) ($\delta^{18}O$) + (0.4) ($\delta^{18}O'$). Positive values indicate good preservation.

just how *state* and *rate of change* are to be defined in terms of oceanography. We suggest that three factors will turn out to be important as the internal driving variables of carbonate preservation: (1) the intensity of the NADW production, which governs the asymmetry in carbonate accumulation between the Atlantic and Pacific (Olausson, 1965; Berger, 1970b); (2) the extent to which shelves trap or release carbonate (Berger and Winterer, 1974; Milliman, 1974); and (3) the productivity level of the ocean, and the partitioning of productivity between coastal and open ocean (Keir and Berger, 1983; Berger and Keir, 1984).

Productivity

G. tumida *vs.* Pulleniatina

The abundance of *G. tumida* relative to the sum of *Pulleniatina* and *G. tumida* is a measure of the degree of upwelling along the equator in the Pacific. The relative dominance of key species changes from east to west along the equator from *Globoquadrina dutertrei,* to *Globorotalia tumida*, and to *Pulleniatina*, when this relationship is not obscured by dominant species in well-preserved samples. Parker and Berger (1971) suggest that this east-west gradient should be useful in paleogeographic reconstruction of the westward extent of the high fertility zone that originates in the eastern tropical Pacific. The ratio of *G. tumida* to the sum of *Pulleniatina* and *G. tumida* (TUM index; Table 2), does indeed show the expected relationship to glacial-interglacial fluctuations in $\delta^{18}O$, with increased abundance of *G. tumida* during glacials (Fig. 10). The match is poor, however, between Stages 14 and 17 (ca. 500–700 ka). Also, for the last 200 k.y., the match is not good. Amplitudes of the TUM signal are uncommonly large from 15 mbsf downward, where obliquity cycles begin to dominate.

Benthic Foraminifer Abundance

The accumulation rate of benthic foraminifers in the sediments of the Ontong Java Plateau can be used to reconstruct glacial-to-interglacial changes in productivity (Herguera and Berger, 1991). Unfortunately, accumulation rates are not easily obtained on the relevant scale of variation because instantaneous accumulation rates are sensitive to small errors in successive age assignments. Here we use the total number of benthic foraminifers per gram of dry sediment (BF/g index) (Table 2) to track changes in productivity (in fact assuming that sedimentation rates do not vary much downcore). As expected from previous studies (Herguera and Berger, 1991; Burke et al., in press), the abundance of total benthic foraminifers is higher during glacial intervals than during interglacials (Fig. 11). Benthic foraminifers can be concentrated by the effects of differential dissolution, in poorly preserved samples (Parker and Berger, 1971). However, the generally higher abundance of benthic foraminifers during glacials in association with better preservation suggests that benthic abundance is not significantly affected by dissolution in the record at hand. It seems unlikely that higher fluxes of organic matter associated with increased productivity would be sufficient to concentrate the dissolution-resistant benthic foraminifers because foraminifers are better preserved during glacials when benthic foraminifers are more abundant. Qualitatively, the match is quite good, the coincidence of phase being remarkable back to about 1 Ma (ca. 16 mbsf). In detail, mismatches in amplitude are common. Stage 6 shows abundances that are much too great, whereas Stages 10, 12, 14, and 16 show much reduced abundances of benthic foraminifers. Taking the changes in accumulation rate into account (as deduced from counting obliquity cycles; see below) could ameliorate these mismatches. However, this seems unlikely for the lower part of the section. Because of the uncertainty surrounding sedimentation rate determination for short intervals (cf. Berger et al., this volume), we have chosen not to calculate accumulation rates for benthic foraminifers in this report.

Comparisons of Indexes

The correspondence between the two productivity indexes TUM and BF/g is only moderately good; indeed, striking mismatches are evident in places (Fig. 12). The most glaring example is the period around late Stage 7, where the BF/g index exhibits a remarkable excursion that is in no way reflected in the TUM record. The period after that time shows large positive discrepancies of the BF/g values as well. Earlier we noted the unusually high sand content in these sediments. Winnowing should affect BF/g but not TUM. Also, differential dissolution effects must be considered.

At this juncture, we have no reason to prefer one index over the other. Thus, we combine them into one productivity index, CPI (being the mean of two standardized productivity values, standardized), and compare this index with the original $\delta^{18}O$ record (Fig. 13). The correspondence is moderately good, with the mismatches noted earlier persisting.

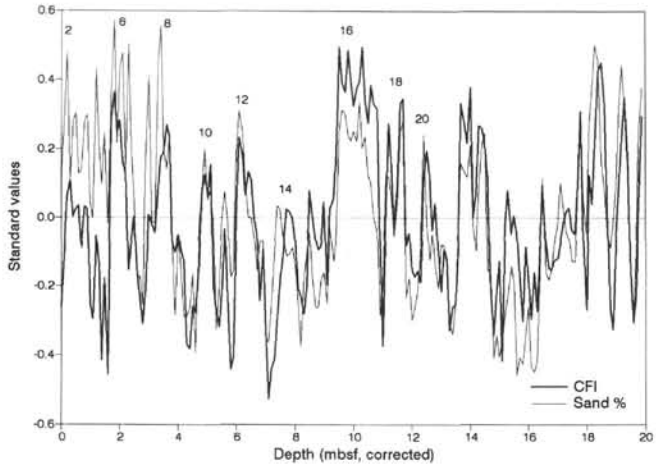

Figure 7. Standardized CFI and standardized percent sand vs. corrected depth. Percent sand is the dry weight percent of particles >63 µm. Positive values indicate good preservation.

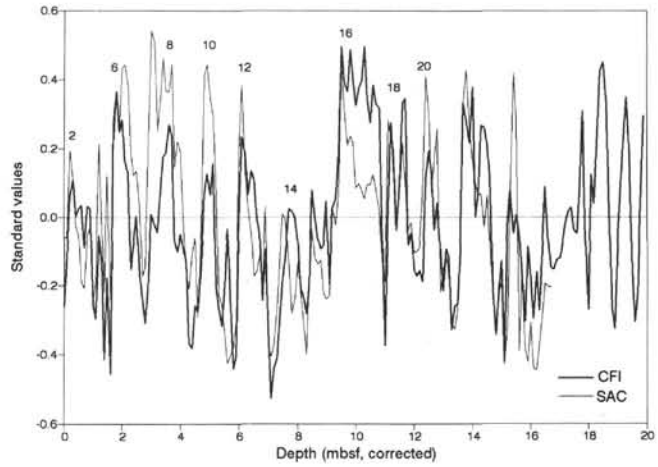

Figure 8. Standardized CFI and standardized abundance of dissolution susceptible species (SAC) vs. corrected depth. The SAC ratio used here is the number of whole tests of *G. sacculifer*/(*G. sacculifer* + *Pulleniatina* + *G. tumida* + *G. menardii*). Positive values indicate good preservation.

It has been suggested repeatedly that carbonate dissolution depends to some degree on the supply of organic matter to the seafloor (e.g., Berger, 1970b; Emerson and Bender, 1981; Archer, 1991). If this is important in our sample set, we should find a strong *negative* correlation between productivity and preservation. Comparing the two available indexes (CPI and CDI), we find that they are in fact positively correlated over much of the record (Fig. 14). However, this correspondence is much weaker than that of the CDI with the $\delta^{18}O$ record. In fact, adding CPI as a third factor into an equation such as Equation (4) yields no improvement of the estimate of the intensity of dissolution. Thus, whatever contribution productivity (as measured by our indexes) makes to the variability of preservation, it is already contained in the fluctuations of the $\delta^{18}O$ values of *Pulleniatina*. Although these observations do not rule out productivity effects on preservation, they suggest that productivity plays a subordinate role (leaving bottom-water saturation as the chief controlling factor).

DISCUSSION

Comparison with Hole 806B

It has long been realized that the pelagic $\delta^{18}O$ record is altered by differential dissolution (reviewed in Wu and Berger, 1991). The sense of this effect is such as to enrich an assemblage in ^{18}O-rich individuals by removal of the more open-structured specimens that made their shells in warm, shallow water. This effect will automatically ensure some correlation between the record of dissolution and that of $\delta^{18}O$, which should oppose the normal glacial-interglacial relationship (k_1 in Eq. 4) but reinforce the one tied to change (k_2 in Eq. 4). To obtain the magnitude of the effect, one has to compare two records taken at different depths along the flanks of the plateau, as did Shackleton and Opdyke (1976). The shallower of the two records can serve as a standard against which to measure the deviation in the deeper one, a difference that can then be ascribed to the effects of differential dissolution. Unfortunately, when matching the cores based on their dissolution-susceptible signals, phase information tends to be lost or distorted (Wu et al., 1990).

The first step in preparing a comparison of two cores is to adjust the depth of one core in synchroneity with that of the other by finding the sedimentation rate ratios (SRRs) between the two cores. We use the percent sand records in Holes 805C (Table 1) and 806B (Table 4) to make the necessary correlation (Fig. 15). A first crude visual fit is achieved by applying the SRR coefficients 1.41, 1.05, and 1.15 to the depth segments of Hole 805C shown in the Figure 15. The presence of a coring gap of about 60 cm then becomes evident in Hole 806B. A similar gap was reported by Berger et al. (this volume) based on matching isotopes and on a visual check using GRAPE data. The percent sand values for Hole 805C are seen to be generally (but not invariably) lower than the corresponding values in Hole 806B, as expected if sand content tracks dissolution history. Peak sand content in Hole 806B is associated with glacial stages and is higher in many instances relative to Hole 805C. Periods of increased winnowing during glacial time (Wu and Berger, 1991) should exhibit amplified differences between percent sand at these sites as fines removed from shallower sites are transported to deeper sites. In this context, increased bioturbation (bio-resuspension) from increased productivity or an increase in deep-sea tidal energy, or both, may be considered as possible causes of winnowing.

The sand-based crude match results in a remarkably good fit of negative *G. sacculifer* $\delta^{18}O$ values (Fig. 16). On the whole, $\delta^{18}O$ values in Hole 806B tend to be slightly more negative than those in Hole 805C, as expected based on the effects of differential dissolution. Within the species *G. sacculifer,* specimens living in shallow water tend to be thin walled and highly porous. Thick-walled terminal morphologies are produced in deeper and colder waters. With dissolution, the selective removal of isotopically light variants of *G. sacculifer* occurs. The effect is expressed preferentially during the interglacials (labeled with their isotope stages), confirming the observation that dissolution is more important during these intervals. The magnitude of the effect is typically <0.2‰, but it can reach up to about 0.3‰. One important result of the $\delta^{18}O$ match is that the Hole 805C record remains trustworthy as a guide to the state of the system, despite interference from dissolution. However, between isotopic Stages 10 and 18, the Hole 805C *Pulleniatina* $\delta^{18}O$ record is also offset toward heavier values during glacials. This suggests that a process other than dissolution may be affecting the *Pulleniatina* record, perhaps related to distance from the equator. Of course, little or nothing can be said about phase shifts between these two records unless a means exists to produce a detailed correlation independent of the signals compared.

Encouraged by the ease with which a good match is achieved between the two records, we next turn to greater detail, attempting peak-to-peak correlation using standardized SAND values (Figs. 17A-17B and 18). The matching was achieved by means of a visual fit of peaks and valleys. A conversion factor for the depth in Hole 805C was assigned to each sample in Hole 806B as the fit was made downcore. From this, the differentials between adjacent samples in Hole 806B were calculated. This matching function, the

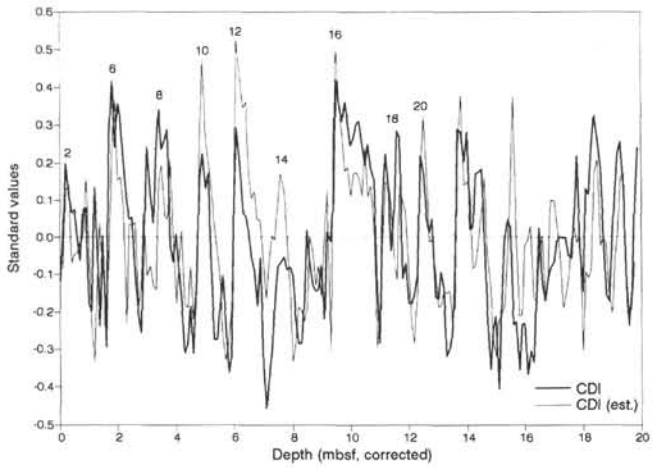

Figure 9. Standardized composite dissolution index (CDI) and standardized CDI (estimated) vs. corrected depth. CDI = (0.5) (CFI) + (0.25) (% SAND) + (0.25) (SAC). CDI (est.) uses $k_1 = 0.55$ and $k_2 = 0.45$ in Equation 4 (described in text). Positive values indicate good preservation.

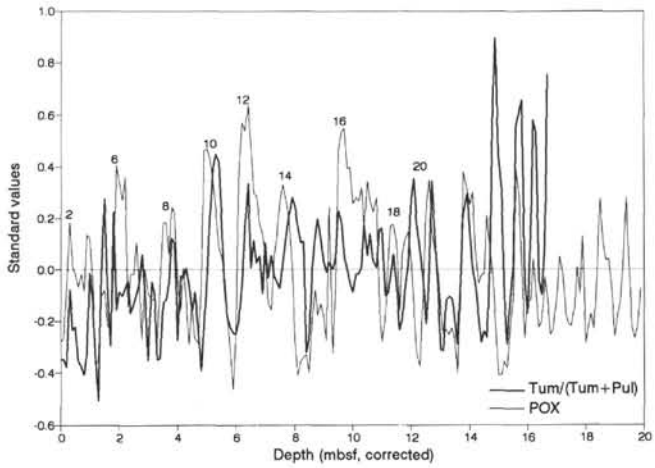

Figure 10. Standardized ratio of number of tests of *G. tumida*/(*Pulleniatina* + *G. tumida*) and standardized $\delta^{18}O$ *Pulleniatina* (POX) vs. corrected depth. Positive values indicate higher productivity.

sequence of instantaneous sedimentation rate ratios (ISRRs), is seen to more or less follow the "crude fit" values proposed earlier but with strong episodic excursions (Fig. 18). Such excursions are produced when matching neighboring peaks in an ad hoc fashion. A Fourier fit to the initial ISRR record removes much of the high-frequency signal and retains the main features of the matching process (Fig. 19). The Fourier fit with 20 harmonics (wavelength = 1 m) is retained for comparison with other variables.

The ISRR record that results from matching and smoothing may be compared with the correspondingly filtered $\delta^{18}O$ record, to check for the effects of glacial-interglacial fluctuations on time scales >70 k.y. The comparison (Fig. 20) shows that no clear relationship exists between the variables. For the uppermost 4 m (ca. 280 ka), we find that the ISRR between the two sites varies such that Hole 806B has a much greater rate of accumulation during glacials. For earlier periods, on the whole, exactly the reverse is indicated.

An analogous comparison of the ISRR record with the CDI signal from Hole 805C (Fig. 21) yields somewhat similar observations in terms of phase reversals. The last 250 k.y. are characterized by high sedimentation rate ratios whenever preservation is good. For the 500 k.y. before that, the phase is reversed (down to 11 mbsf), and a reversed phase is also common below that depth in the hole. However, below 8 mbsf (before 500 ka), a tendency exists for long-term trends to be in phase, in the sense that good preservation in Hole 805C means disproportionately high sedimentation rates in Hole 806B, and vice versa. A priori, one might expect that increased dissolution in Hole 805C should increase the ISRR between Holes 806 and 805, if the effects of dissolution do not reach up to shallower depths. Thus, the last 250 k.y. would represent the anomalous situation. Unusually high productivity fluctuations (as suggested by the TUM index), combined with unusually strong glacial winnowing activity (as suggested by sand content), may contain the answers to this question.

Based on the 41-k.y. $\delta^{18}O$ spacing shown in Figure 3, average sedimentation rates per 41-k.y. increment were calculated (Fig. 22). Any partial cycles at the top and bottom of the studied interval were assigned sedimentation rate values based on adjacent complete intervals. The 41-k.y. step-function sedimentation rates were smoothed by constructing a Fourier fit using the first 20 harmonics, and the resulting instantaneous sedimentation rates were used to transform the depth series into a time series (Table 3). This analysis of Hole 805C places the Brunhes/Matuyama boundary near 830,000 ka rather than near 790,000 ka (Shackleton et al., 1990; Izett and Obradovich, 1991; Berger et al., this volume).

Significance of the Age Model

The Hole 805C age model of Berger et al. (this volume) is based on data and procedures identical to ours. Instantaneous sedimentation rates (ISRs) estimated here and by Berger et al. (this volume) are shown in Figure 23 for comparison. Note that Berger et al. show both lower and higher ISRs between 2 and 4 mbsf but much higher ISRs near 11 mbsf. The discrepancies between 2 and 4 mbsf cancel for the long term, but those near 11 mbsf do not (Table 3). The discrepancy at 11 mbsf may be explained by the presence of an additional obliquity cycle in our age model, which reduces the ISR in this interval relative to the Berger et al. value. The ISR difference between 2 and 4 mbsf arises despite the fact that data and algorithms are identical. This study treated the entire depth-series as one continuous unit; whereas, Berger et al. treated each core as a separate unit and added synthetic data to the extrapolated ends of each data set. Berger et al. combine the $\delta^{18}O$ records of *Pulleniatina* and *G. sacculifer* for generation of the obliquity-related cycles; we use only the *Pulleniatina* record, however. Also, the age model used here avoids the discrepancies in age assignments that arise when comparing counts from obliquity and eccentricity cycles at 0.9 to 1 Ma, as noted by Berger et al. (this volume).

A test for the two age models and the resulting ISRs in this work might be derived from dissolution patterns. Higher ISRs should be associated with better preservation if preservation is important to net sedimentation rate. However, comparison of our ISRs with CDI (Fig. 24) shows that our ISR model does not consistently respond to observed CDI, making such a test inconclusive.

CONCLUSIONS

Our results confirm previous observations associating periods of enhanced preservation with glacial periods and with glacial-to-interglacial transitions. In particular, our results show that the record of dissolution is best reconstructed when the state and rate of change of the system based on $\delta^{18}O$ *Pulleniatina* are considered. Accounting for the effects of productivity do not improve the estimate of the intensity of dissolution, suggesting that whatever contribution productivity makes to the variability of preservation, it is already contained in the fluctuations of the $\delta^{18}O$ values of *Pulleniatina*. Measurements of our productivity indexes suggest that productivity plays a subordinate role in foraminiferal carbonate dissolution, leaving bottom-water saturation as the chief controlling factor. However, a straightforward correlation between the record of preservation and the sedimentation

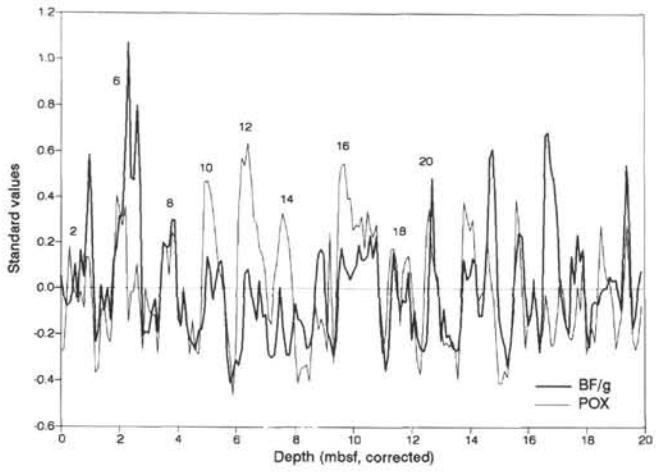

Figure 11. Standardized total number of benthic foraminifers per gram of dry sediment (BF/g) and standardized $\delta^{18}O$ *Pulleniatina* (POX) vs. corrected depth. Positive values indicate higher productivity.

rate stratigraphy of these carbonate-rich sediments could not be established. Also, notable differences are present between the responses of individual dissolution indexes pointing to the variable importance of other processes, which include (but are not limited to) winnowing, bioturbation, and productivity.

ACKNOWLEDGMENTS

We thank G. Wefer and T. Bickert, University of Bremen, for permitting use of unpublished isotope data. We also thank the anonymous reviewer for critical and constructive reading of the manuscript and Huy Tran for careful sample preparation. This work was supported through National Science Foundation Grant No. OCE 90-17717 and U.S. Science Support Program Purchase Order No. 20461.

REFERENCES

Adelseck, C.G., Jr., 1977. Recent and late Pleistocene sediments from the eastern equatorial Pacific Ocean: sedimentation and dissolution [Ph.D. dissert.]. Univ. of California, San Diego.

Adelseck, C.G., Jr., and Anderson, T.F., 1978. The late Pleistocene record of productivity fluctuations in the eastern equatorial Pacific Ocean. *Geology,* 6:388–391.

Archer, D., 1991. Modeling the calcite lysocline. *J. Geophys. Res.*, 96:17,037–17,050.

Arrhenius, G., 1952. Properties of the sediment and their distribution: sediment cores from the East Pacific. *Rep. Swed. Deep-Sea Exped. 1947–1948,* 5:12–23.

———, 1988. Rate of production, dissolution and accumulation of biogenic solids in the ocean. *Palaeogeogr., Palaeoclimatol., Palaeoecol.,* 67:119–146.

Berger, W.H., 1970a. Planktonic foraminifera: selective solution and the lysocline. *Mar. Geol.,* 8:111–138.

———, 1970b. Biogenous deep-sea sediments: fractionation by deep-sea circulation. *Geol. Soc. Am. Bull.,* 81:1385–1402.

———, 1973. Deep-sea carbonates: Pleistocene dissolution cycles. *J. Foraminiferal Res.,* 3:187–195.

———, 1977. Carbon dioxide excursions and the deep sea record: aspects of the problem. *In* Andersen, N.R., and Malahoff, A. (Eds.), *The Fate of Fossil Fuel CO_2 in the Oceans:* New York (Plenum), 505–542.

———, 1992. Pacific carbonate cycles revisited: arguments for and against productivity control. *In* Ishizaki, K., and Saito, T. (Eds.), *Centenary of Japanese Micropaleontology:* Tokyo (Terra Sci.), 15–25.

Berger, W.H., and Keir, R.S., 1984. Glacial-Holocene changes in atmospheric CO_2 and the deep-sea record. *In* Hansen, J.E., and Takahashi, T. (Eds.), *Climate Processes and Climate Sensitivity.* Am. Geophys. Union, Maurice Ewing Ser., 5:337–351.

Berger, W.H., Kroenke, L.W., Mayer, L.A., and Shipboard Scientific Party, 1991. Ontong Java Plateau, Leg 130: synopsis of major drilling results. *In* Kroenke, L.W., Berger, W.H., Janecek, T.R., et al., *Proc. ODP, Init. Repts.,* 130: College Station, TX (Ocean Drilling Program), 497–537.

Berger, W.H., and Vincent, E., 1981. Chemostratigraphy and biostratigraphic correlation: exercises in systemic stratigraphy. *Oceanol. Acta, Suppl.,* 4:115–127.

Berger, W.H., and Winterer, E.L., 1974. Plate stratigraphy and the fluctuating carbonate line. *In* Hsü, K.J., and Jenkyns, H.C. (Eds.), *Pelagic Sediments on Land and Under the Sea.* Spec. Publ. Int. Assoc. Sedimentol., 1:11–48.

Broecker, W.S., and van Donk, J., 1970. Insolation changes, ice volumes and the ^{18}O record in deep-sea sediments. *Rev. Geophys. Space Phys.,* 8:169–198.

Burke, S.K., Berger, W.H., Coulbourn, W.T., and Vincent, E., in press. Benthic foraminifera in Box Core ERDC 112, Ontong Java Plateau. *J. Foraminiferal Res.*

Chuey, J.M., Rea, D.K., and Pisias, N.G., 1987. Late Pleistocene paleoclimatology of the central equatorial Pacific: a quantitative record of eolian and carbonate deposition. *Quat. Res.,* 28:323–339.

Crowley, T.J., 1985. Late Quaternary changes in the North Atlantic and Atlantic/Pacific comparison. *In* Sundquist, E.T., and Broecker, W.S. (Eds.), *The Carbon Cycle and the Atmospheric CO_2: Natural Variations Archean to Present.* Am. Geophys. Union Monogr., 32:271–284.

Emerson, S., and Bender, M., 1981. Carbon fluxes at the sediment-water interface of the deep-sea: calcium carbonate preservation. *J. Mar. Res.,* 39:139–162.

Farrell, J.W., and Prell, W.L., 1989. Climatic change and $CaCO_3$ preservation: an 800,000 year bathymetric reconstruction from the central equatorial Pacific Ocean. *Paleoceanography,* 4:447–466.

———, 1991. Pacific $CaCO_3$ preservation and $\delta^{18}O$ since 4 Ma: paleoceanic and paleoclimatic implications. *Paleoceanography,* 6:485–498.

Gardner, J.V., 1982. High-resolution carbonate and organic-carbon stratigraphies for the late Neogene and Quaternary from the western Caribbean and eastern equatorial Pacific. *In* Prell, W.L., Gardner, J.V., et al., *Init. Repts. DSDP,* 68: Washington (U.S. Govt. Printing Office), 347–364.

Grötsch, J., Wu, G., and Berger, W.H., 1991. Carbonate cycles in the Pacific: reconstruction of saturation fluctuations. *In* Einsele, G., Ricken, W., and Seilacher, A. (Eds.), *Cycles and Events in Stratigraphy:* Heidelberg (Springer-Verlag), 110–125.

Hays, J.D., Saito, T., Opdyke, N.D., and Burckle, L.H., 1969. Pliocene-Pleistocene sediments of the equatorial Pacific: their paleomagnetic, biostratigraphic, and climate record. *Geol. Soc. Am. Bull.,* 8:1481–1514.

Hebbeln, D., Wefer, G., and Berger, W.H., 1990. Pleistocene dissolution fluctuations from apparent depth of deposition in Core ERDC-127P, west-equatorial Pacific. *Mar. Geol.,* 165–176.

Herguera, J.C., and Berger, W.H., 1991. Productivity from benthic foraminifera abundance: glacial to postglacial change in the west-equatorial Pacific. *Geology,* 19:1173–1176.

Imbrie, J., Hays, J.D., Martinson, D.G., McIntyre, A., Mix, A.C., Morley, J.J., Pisias, N.J., Prell, W.L., and Shackleton, N.J., 1984. The orbital theory of Pleistocene climate: support from a revised chronology of the marine $\delta^{18}O$ record. *In* Berger, A.L., Imbrie, J., Hays, J., Kukla, G., and Saltzman, B. (Eds.), *Milankovitch and Climate* (Pt. 2): Dordrecht (D. Reidel), 269-305.

Izett, G.A., and Obradovich, J.D., 1991. Dating of the Matuyama-Brunhes boundary based on ^{40}Ar-^{39}Ar ages of the Bishop Tuff and Cerro San Luis rhyolite. *Geol. Soc. Am., Abstr. Progr.,* A106.

Johnson, T.C., Hamilton, E.L., and Berger, W.H., 1977. Physical properties of calcareous ooze: control by dissolution at depth. *Mar. Geol.,* 24:259–277.

Keir, R.S., and Berger, W.H., 1983. Atmospheric CO_2 content in the last 120,000 years: the phosphate extraction model. *J. Geophys. Res.,* 88:6027–6038.

Le, J., and Shackleton, N.J., 1992. Carbonate dissolution fluctuations in the western equatorial Pacific during the late Quaternary. *Paleoceanography,* 7:21–42.

Luz, B., and Shackleton, N.J., 1975. $CaCO_3$ solution in the tropical east Pacific during the past 130,000 years. *In* Sliter, W.V., Bé, A.W.H., and Berger, W.H. (Eds.), *Dissolution of Deep-Sea Carbonates.* Spec. Publ. Cushman Found. Foraminiferal Res., 13:142–150.

Lyle, M., Murray, D.W., Finney, B.P., Dymond, J., Robbins, J.M., and Brooksforce, K., 1988. The record of late Pleistocene biogenic sedimentation in the eastern tropical Pacific Ocean. *Paleoceanography,* 3:39–59.

Milliman, J.D., 1974. *Marine Carbonates:* New York (Springer-Verlag).

Moore, T.C., Pisias, N.G., and Dunn, D.A., 1982. Carbonate time series of the Quaternary and late Miocene sediments in the Pacific Ocean: a spectral comparison. *Mar. Geol.,* 46:217–234.

Moore, T.C., Pisias, N.G., and Heath, G.R., 1977. Climate changes and lags in Pacific carbonate preservation, surface temperature and global ice volume. *In* Anderson, N.R., and Malahoff, A. (Eds.), *The Fate of Fossil Fuel CO_2 in the Oceans:* New York (Plenum), 145–165.

Olausson, E., 1965. Evidence of climatic changes in North Atlantic deep-sea cores, with remarks on isotopic paleotemperature analysis. *Prog. Oceanogr.*, 3:221–252.

Parker, F.L., and Berger, W.H., 1971. Faunal and solution patterns of planktonic Foraminifera in surface sediments of the South Pacific. *Deep-Sea Res., Pt. A,* 18:73–107.

Peterson, L.C., and Prell, W.L., 1985a. Carbonate preservation and rates of climatic change: an 800 kyr record from the Indian Ocean. *In* Sundquist, E.T., and Broecker, W.S. (Eds.), *The Carbon Cycle and Atmospheric CO_2: Natural Variations Archean to Present.* Am. Geophys. Union Monogr., 32:251–270.

————, 1985b. Carbonate dissolution in recent sediments of the eastern equatorial Indian Ocean: preservation patterns and carbonate loss above the lysocline. *Mar. Geol.,* 64:259–290.

Pisias, N.G., 1976. Late Quaternary sediment of the Panama Basin: sedimentation rates, periodicities, and controls of carbonate and opal accumulation. *Mem.—Geol. Soc. Am.,* 145:375–391.

Price, B.A., 1988. Equatorial Pacific sediments: a chemical approach to ocean history [Ph.D. dissert.]. Univ. of California, San Diego.

Schiffelbein, P., 1984. Stable isotope systematics in Pleistocene deep-sea sediment records [Ph.D dissert.]. Univ. of California, San Diego.

Schiffelbein, P., and Dorman, L., 1986. Spectral effects of time-depth nonlinearities in deep sea sediments records: a demodulation technique for realigning time and depth scales. *J. Geophys. Res.,* 91:3821–3835.

Shackleton, N.J., 1977. Carbon-13 in *Uvigerina:* tropical rainforest history and the equatorial Pacific carbonate dissolution cycles. *In* Andersen, N.R., and Malahoff, A. (Eds.), *The Fate of Fossil Fuel CO_2 in the Oceans:* New York (Plenum), 401–427.

Shackleton, N.J., Berger, A., and Peltier, W.R., 1990. An alternative astronomical calibration of the lower Pleistocene timescale based on ODP Site 677. *Trans. R. Soc. Edinburgh, Earth Sci.,* 81:251–261.

Shackleton, N.J., and Opdyke, N.D., 1973. Oxygen isotope and palaeomagnetic stratigraphy of equatorial Pacific Core V28-238: oxygen isotope temperatures and ice volumes on a 10^5 year and 10^6 year scale. *Quat. Res.,* 3:38–55.

————, 1976. Oxygen-isotope and paleomagnetic stratigraphy of Pacific core V28-239 Late Pliocene to latest Pleistocene. *Mem.—Geol. Soc. Am.,* 145:449–464.

Shipboard Scientific Party, 1991. Site 805. *In* Kroenke, L.W., Berger, W.H., Janecek, T.R., et al., *Init. Repts. ODP,* 130: College Station, TX (Ocean Drilling Program), 223–290.

Thompson, P.R., 1976. Planktonic foraminiferal dissolution and the progress towards a Pleistocene equatorial Pacific transfer function. *J. Foraminiferal Res.,* 6:208–227.

Thompson, P.R., and Saito, T., 1974. Pacific Pleistocene sediments: planktonic foraminifera dissolution cycles and geochronology. *Geology,* 2:333–335.

Thunell, R.C., 1976. Optimum indices of calcium carbonate dissolution in deep-sea sediments. *Geology,* 4:525–528.

Valencia, M., 1977. Pacific Pleistocene paleoclimatic stratigraphies: a comparative analysis of results. *Quat. Res.,* 8:339–354.

Vincent, E., 1985. Distribution stratigraphique de la teneur en carbonate dans les sédiments néogènes et quaternaires de l'océan Pacifique. *Bull. Soc Geol. Fr.,* 8:915–924.

Volat, J.L., Pastouret, L., and Vergnaud-Grazzini, C., 1980. Dissolution and carbonate fluctuations in Pleistocene deep-sea cores: a review. *Mar. Geol.,* 34:1–28.

Wu, G., and Berger, W.H., 1989. Planktonic foraminifera: differential dissolution and the Quaternary stable isotope record in the west equatorial Pacific. *Paleoceanography,* 4:181–198.

————, 1991. Pleistocene ^{18}O record from Ontong-Java Plateau: effects of winnowing and dissolution. *Mar. Geol.,* 96:193–209.

Wu, G., Herguera, J.C., and Berger, W.H., 1990. Differential dissolution: modification of late Pleistocene oxygen isotope records in the western equatorial Pacific. *Paleoceanography,* 5:581–594.

Wu, G., Yasuda, M.K., and Berger, W.H., 1991. Late Pleistocene carbonate stratigraphy on Ontong-Java Plateau in the western equatorial Pacific. *Mar. Geol.,* 99:135–150.

Date of initial report: 21 February 1992
Date of acceptance: 7 September 1992
Ms 130B-008

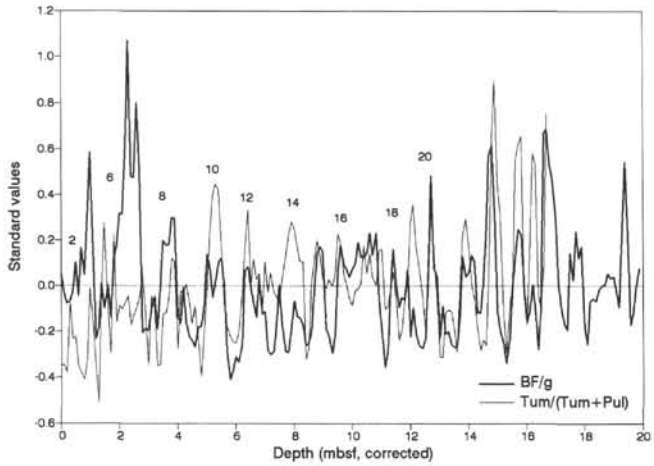

Figure 12. Comparison of productivity indexes: standardized whole tests of *G. tumida*/(*Pulleniatina* + *G. tumida*) and standardized total number of benthic foraminifers per gram of dry sediment (BF/g) vs. corrected depth. Positive values indicate higher productivity.

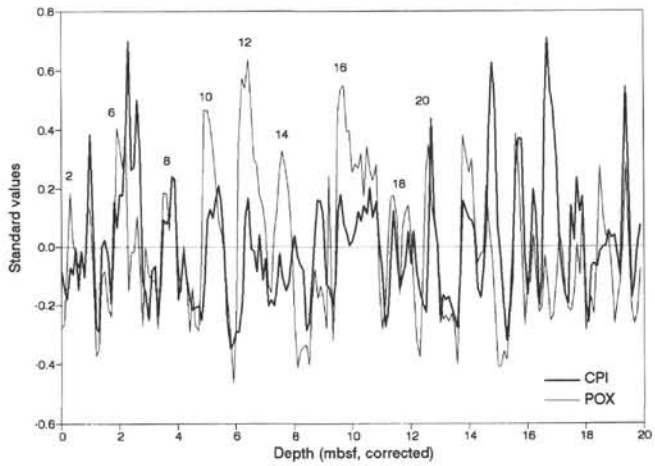

Figure 13. Standardized composite productivity index (CPI) and standardized $\delta^{18}O$ *Pulleniatina* (POX) vs. corrected depth. CPI is the standardized mean of the two standardized productivity indexes, *G. tumida*/(*Pulleniatina* + *G. tumida*), and total number of benthic foraminifers per gram of dry sediment (BF/g). Positive CPI values indicate higher productivity.

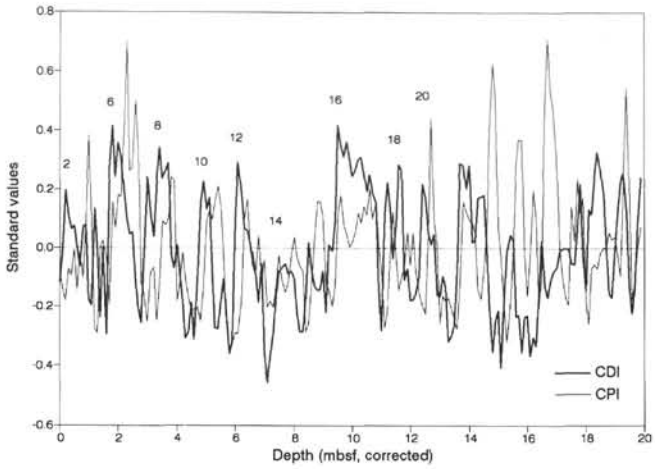

Figure 14. CDI and CPI vs. corrected depth.

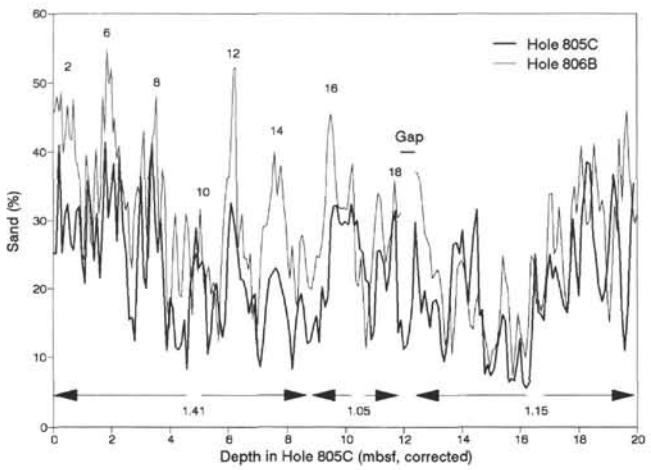

Figure 15. Percent sand at Holes 805C and 806B correlated to corrected depth of Hole 805C based on linear fit within three separate depth ranges. Values 1.41, 1.05, and 1.15 are sedimentation rate ratios (SRR) applied to depth segments of Hole 805C for correlation with Hole 806B. Note that a gap must be postulated for Hole 806B to obtain this fit.

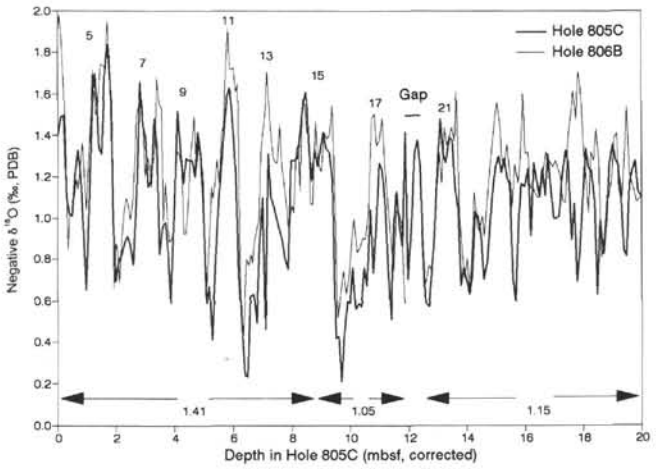

Figure 16. Negative $\delta^{18}O$ *G. sacculifer* at Holes 805C and 806B correlated by matching percent sand as shown in Figure 15.

Table 4. Percent sand (>63 μm) by dry weight, Hole 806B.

Core, section, interval (cm)	Depth* (mbsf)	Sand fraction >63 μm (%)	Core, section, interval (cm)	Depth* (mbsf)	Sand fraction >63 μm (%)	Core, section, interval (cm)	Depth* (mbsf)	Sand fraction >63 μm (%)
1H-1, 9–11	0.09	45.8	2H-1, 59–61	7.09	31.9	2H-5, 108–110	13.58	42.5
1H-1, 19–21	0.19	48.3	2H-1, 69–71	7.19	27.0	2H-5, 119–121	13.69	33.5
1H-1, 29–31	0.29	45.3	2H-1, 79–81	7.29	20.6	2H-5, 129–131	13.79	31.9
1H-1, 39–41	0.39	50.1	2H-1, 89–91	7.39	19.9	2H-5, 139–141	13.89	31.7
1H-1, 49–51	0.49	40.2	2H-1, 99–101	7.49	24.3	2H-5, 148–150	13.98	32.0
1H-1, 59–61	0.59	41.4	2H-1, 109–111	7.59	21.1	2H-6, 9–11	14.09	31.6
1H-1, 69–71	0.69	46.8	2H-1, 119–121	7.69	18.5	2H-6, 19–21	14.19	33.1
1H-1, 79–81	0.79	44.3	2H-1, 129–131	7.79	22.3	2H-6, 29–31	14.29	42.0
1H-1, 89–91	0.89	38.5	2H-1, 139–141	7.89	19.8	2H-6, 36–38	14.36	28.5
1H-1, 99–101	0.99	48.7	2H-1, 148–150	7.98	15.8	2H-6, 49–51	14.49	19.9
1H-1, 109–111	1.09	41.8	2H-2, 9–11	8.09	12.2	2H-6, 59–61	14.59	23.1
1H-1, 119–121	1.19	36.8	2H-2, 19–21	8.19	22.7	2H-6, 69–71	14.69	23.8
1H-1, 129–131	1.29	39.8	2H-2, 29–31	8.29	28.7	2H-6, 79–81	14.79	13.3
1H-1, 139–141	1.39	30.5	2H-2, 39–41	8.39	33.6	2H-6, 89–91	14.89	12.5
1H-1, 148–150	1.48	23.4	2H-2, 49–51	8.49	36.3	2H-6, 99–101	14.99	21.6
1H-2, 9–11	1.59	28.2	2H-2, 59–61	8.59	35.1	2H-6, 108–110	15.08	24.1
1H-2, 19–21	1.69	45.2	2H-2, 69–71	8.69	43.1	2H-6, 119–121	15.19	31.4
1H-2, 29–31	1.79	29.4	2H-2, 79–81	8.79	47.1	2H-6, 129–131	15.29	34.3
1H-2, 39–41	1.89	27.1	2H-2, 89–91	8.89	59.1	2H-6, 139–141	15.39	32.9
1H-2, 49–51	1.99	26.6	2H-2, 99–101	8.99	30.7	2H-6, 148–150	15.48	28.2
1H-2, 59–61	2.09	36.7	2H-2, 109–111	9.09	25.5	2H-7, 9–11	15.59	23.8
1H-2, 69–71	2.19	40.4	2H-2, 119–121	9.19	33.8	2H-7, 19–21	15.69	26.9
1H-2, 79–81	2.29	29.7	2H-2, 129–131	9.29	24.7	2H-7, 27–29	15.77	25.9
1H-2, 89–91	2.39	33.7	2H-2, 139–141	9.39	26.1	2H-7, 39–41	15.89	36.2
1H-2, 99–101	2.49	48.0	2H-2, 148–150	9.48	23.4	2H-7, 49–51	15.99	30.9
1H-2, 108–110	2.58	41.6	2H-3, 9–11	9.59	23.1	2H-7, 59–61	16.09	30.4
1H-2, 119–121	2.69	55.0	2H-3, 19–21	9.69	25.5	2H-7, 67–69	16.17	33.6
1H-2, 129–131	2.79	49.2	2H-3, 29–31	9.79	12.6	3H-1, 9–11	16.09	36.5
1H-2, 139–141	2.89	53.9	2H-3, 39–41	9.89	18.9	3H-1, 19–21	16.19	32.4
1H-2, 148–150	2.98	42.4	2H-3, 49–51	9.99	10.9	3H-1, 39–41	16.39	26.6
1H-3, 9–11	3.09	46.4	2H-3, 59–61	10.09	17.8	3H-1, 49–51	16.49	28.3
1H-3, 19–21	3.19	38.4	2H-3, 69–71	10.19	23.8	3H-1, 59–61	16.59	21.3
1H-3, 29–31	3.29	42.3	2H-3, 79–81	10.29	28.9	3H-1, 69–71	16.69	23.7
1H-3, 39–41	3.39	36.5	2H-3, 89–91	10.39	29.1	3H-1, 79–81	16.79	20.2
1H-3, 49–51	3.49	36.4	2H-3, 99–101	10.49	29.2	3H-1, 89–91	16.89	25.1
1H-3, 59–61	3.59	30.4	2H-3, 109–111	10.59	31.1	3H-1, 99–101	16.99	19.8
1H-3, 69–71	3.69	34.2	2H-3, 119–121	10.69	33.7	3H-1, 107–109	17.07	18.5
1H-3, 79–81	3.79	28.7	2H-3, 129–131	10.79	36.2	3H-1, 118–120	17.18	11.2
1H-3, 89–91	3.89	23.0	2H-3, 139–141	10.89	40.0	3H-1, 129–131	17.29	13.9
1H-3, 99–101	3.99	25.0	2H-3, 148–150	10.98	38.2	3H-1, 139–141	17.39	18.4
1H-3, 108–110	4.08	32.6	2H-4, 9–11	11.09	31.2	3H-1, 148–150	17.48	10.4
1H-3, 114–116	4.14	33.1	2H-4, 19–21	11.19	41.9	3H-2, 9–11	17.59	15.7
1H-4, 9–11	4.59	42.8	2H-4, 29–31	11.29	32.7	3H-2, 19–21	17.69	22.4
1H-4, 19–21	4.69	26.9	2H-4, 39–41	11.39	33.1	3H-2, 39–41	17.89	24.7
1H-4, 29–31	4.79	25.0	2H-4, 49–51	11.49	27.7	3H-2, 52–54	18.02	21.7
1H-4, 39–41	4.89	35.5	2H-4, 59–61	11.59	23.0	3H-2, 61–63	18.11	21.8
1H-4, 49–51	4.99	42.3	2H-4, 69–71	11.69	21.4	3H-2, 69–71	18.19	15.8
1H-4, 59–61	5.09	42.6	2H-4, 79–81	11.79	26.8	3H-2, 79–81	18.29	15.2
1H-4, 69–71	5.19	49.8	2H-4, 89–91	11.89	21.7	3H-2, 88–90	18.38	13.9
1H-4, 79–81	5.29	28.1	2H-4, 99–101	11.99	18.4	3H-2, 99–101	18.49	18.6
1H-4, 89–91	5.39	29.5	2H-4, 108–110	12.08	15.6	3H-2, 109–111	18.59	19.1
1H-4, 99–101	5.49	36.6	2H-4, 119–121	12.19	26.5	3H-2, 118–120	18.68	16.8
1H-4, 108–110	5.58	37.5	2H-4, 129–131	12.29	27.9	3H-2, 129–131	18.79	14.9
1H-4, 118–120	5.68	23.4	2H-4, 139–141	12.39	27.1	3H-3, 9–11	19.09	8.2
1H-4, 129–131	5.79	14.4	2H-5, 9–11	12.59	20.3	3H-3, 19–21	19.19	10.8
1H-4, 139–141	5.89	16.3	2H-5, 19–21	12.69	20.8	3H-3, 39–41	19.39	11.5
1H-4, 148–150	5.98	23.4	2H-5, 29–31	12.79	19.3	3H-3, 49–51	19.49	15.3
1H-5, 9–11	6.09	30.3	2H-5, 39–41	12.89	25.9	3H-3, 59–61	19.59	22.1
1H-5, 19–21	6.19	29.4	2H-5, 49–51	12.99	22.7	3H-3, 69–71	19.69	25.3
1H-5, 29–31	6.29	21.8	2H-5, 59–61	13.09	26.6	3H-3, 79–81	19.79	18.7
2H-1, 9–11	6.59	25.0	2H-5, 69–71	13.19	26.9	3H-3, 89–91	19.89	20.9
2H-1, 19–21	6.69	15.9	2H-5, 79–81	13.29	36.2	3H-3, 99–101	19.99	10.8
2H-1, 29–31	6.79	21.8	2H-5, 89–91	13.39	43.8	3H-3, 107–109	20.07	7.2
2H-1, 39–41	6.89	26.7	2H-5, 99–101	13.49	45.3	3H-3, 118–120	20.18	11.4
2H-1, 49–51	6.99	19.7						

*ODP depth assignment = depth has not been adjusted.

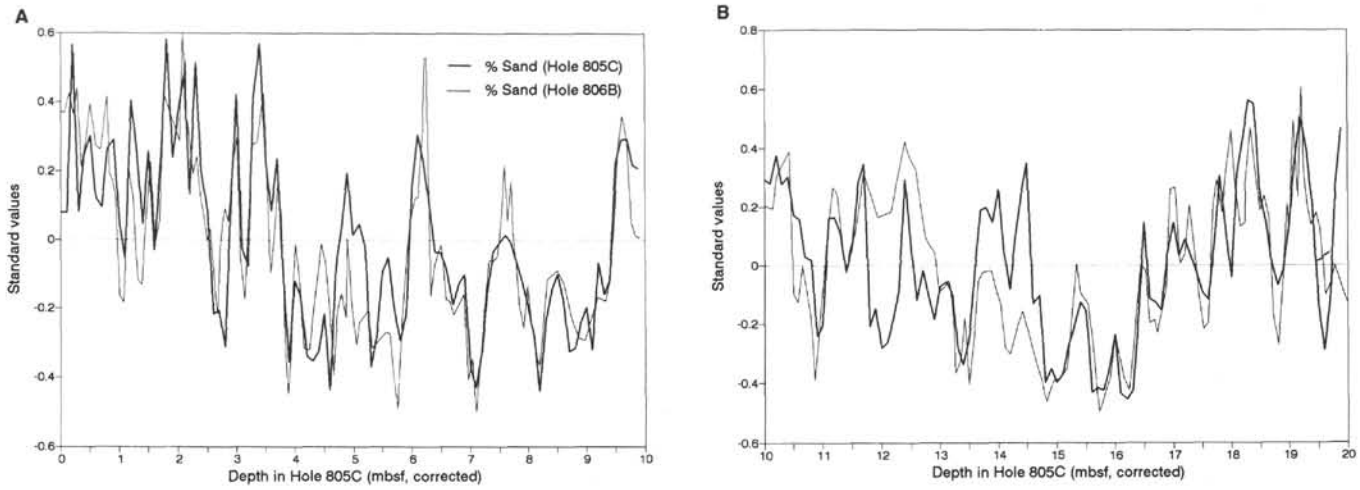

Figure 17. **A, B.** Standardized percent sand, Holes 805C and 806B, with Hole 806B data correlated to corrected depth of Hole 805C using peak-to-peak fit. Figures 17A and 17B show data for 0–10 and 10–20 mbsf (corrected), respectively.

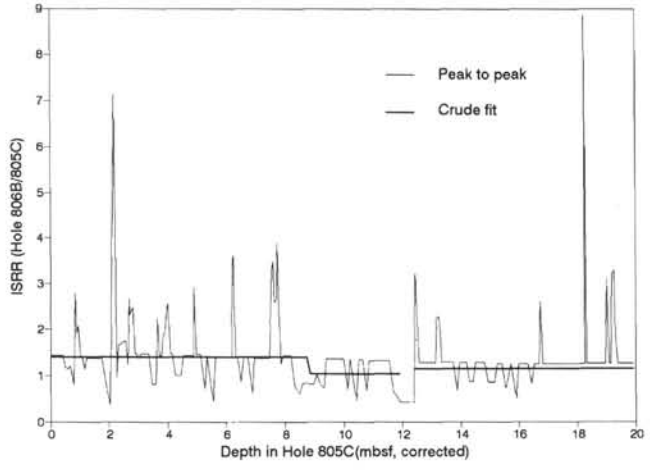

Figure 18. Instantaneous sedimentation rate ratios (ISRR), Holes 806B/ 805C, based on peak-to-peak fit of percent sand records (Figs. 17A–17B) and on crude fit shown in Figure 15 vs. corrected depth for Hole 805C.

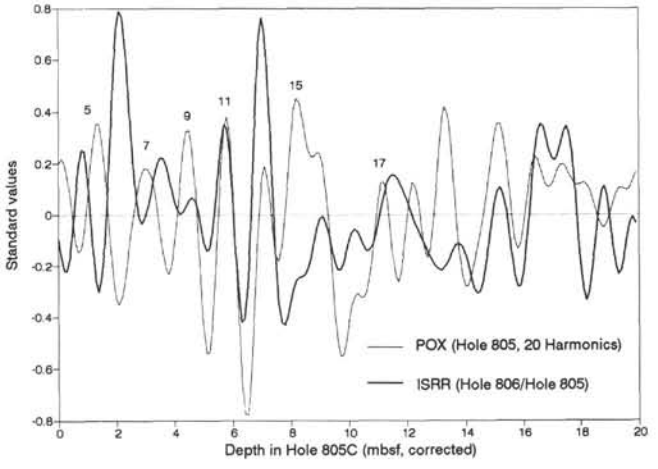

Figure 20. Fourier reconstruction of ISRR Holes 806B/805C (Fig. 19) and $\delta^{18}O$ *Pulleniatina* (both using the first 20 harmonics) vs. corrected depth, Hole 805C.

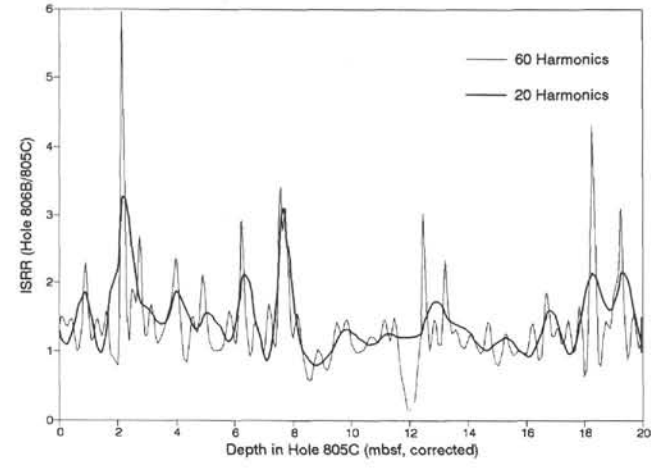

Figure 19. Fourier reconstruction of ISRR Holes 806B/805C, based on peak-to-peak fit (Fig. 18) using the first 60 and 20 harmonics vs. corrected depth for Hole 805C.

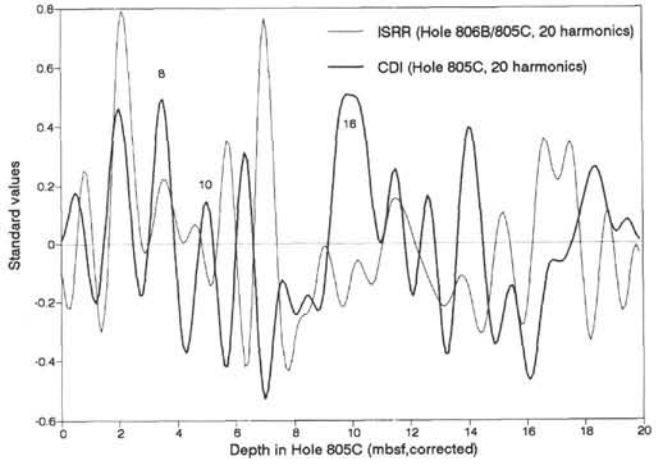

Figure 21. Fourier reconstructions of ISRR Holes 806B/805C (Fig. 19) and CDI (both using the first 20 harmonics) vs. corrected depth for Hole 805C. Positive CDI values indicate good preservation.

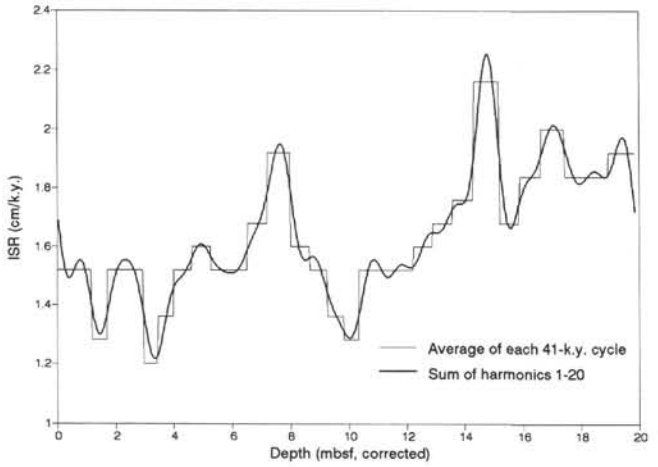

Figure 22. Instantaneous sedimentation rates (ISR) for Hole 805C based on counting 41-k.y. cycles (Fig. 3). The figure shows both the average sedimentation rate per 41-k.y. cycle and the Fourier fit of this curve using the first 20 harmonics vs. corrected depth. The association of age with depth based on these instantaneous sedimentation rates is shown in Table 3.

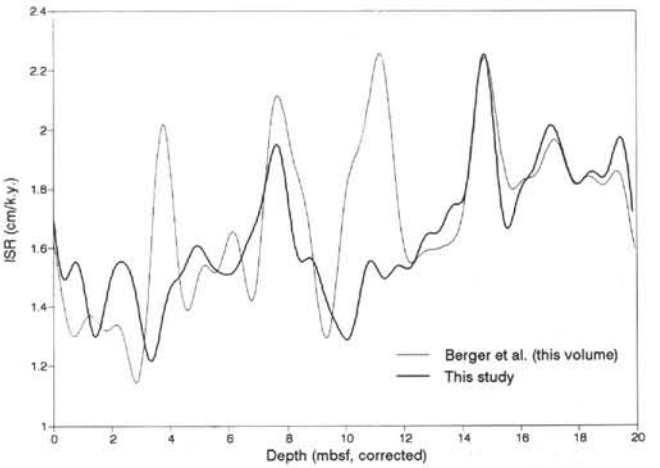

Figure 23. Comparison of instantaneous sedimentation rates (ISR) for Hole 805C resulting from Berger et al. (this volume, using $\delta^{18}O$ *G. sacculifer*) with those of this paper (using $\delta^{18}O$ *Pulleniatina*) vs. corrected depth.

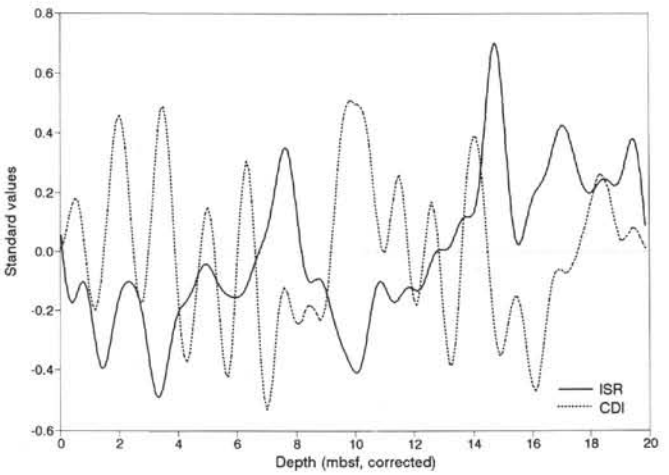

Figure 24. Comparison of instantaneous sedimentation rates (ISR) with CDI for Hole 805C. ISR and CDI plotted vs. corrected depth for Hole 805C.

APPENDIX

Planktonic Foraminiferal Abundances, Hole 805C

Core, section, interval (cm)	Depth* (mbsf)	*Globigerinoides sacculifer* (#/gm)	*Pulleniatina* (#/gm)	*Globorotalia menardii* (#/gm)	*Globorotalia tumida* (#/gm)
1H-1, 13–15	0.13	356	772	71	91
1H-1, 21–23	0.21	251	244	25	25
1H-1, 29–31	0.29	104	121	17	35
1H-1, 39–41	0.39	87	179	15	34
1H-1, 49–51	0.49	142	272	40	55
1H-1, 59–61	0.59	88	302	22	42
1H-1, 69–71	0.69	78	296	48	32
1H-1, 69–71	0.69	71	301	48	33
1H-1, 89–91	0.89	164	314	26	29
1H-1, 89–91	0.89	166	326	23	33
1H-1, 89–91	0.89	168	322	31	24
1H-1, 99–101	0.99	85	211	44	69
1H-1, 109–111	1.09	15	182	37	39
1H-1, 119–121	1.19	120	184	29	47
1H-1, 129–131	1.29	383	346	8	11
1H-1, 143–145	1.43	26	161	22	35
1H-2, 4–6	1.54	127	129	29	72
1H-2, 19–21	1.69	11	154	26	30
1H-2, 29–31	1.79	269	168	94	27
1H-2, 39–41	1.89	341	220	124	130
1H-2, 49–51	1.99	169	143	87	32
1H-2, 49–51	1.99	173	140	75	42
1H-2, 59–61	2.09	425	190	66	52
1H-2, 69–71	2.19	407	190	47	51
1H-2, 79–81	2.29	322	181	70	51
1H-2, 89–91	2.39	340	334	90	100
1H-2, 99–101	2.49	204	254	49	55
1H-2, 109–111	2.59	217	256	82	60
1H-2, 119–121	2.69	124	180	50	49
1H-2, 129–131	2.79	41	147	23	41
1H-2, 148–150	2.98	102	190	69	71
1H-3, 9–11	3.09	562	219	32	22
1H-3, 19–21	3.19	419	147	49	34
1H-3, 19–21	3.19	432	140	43	37
1H-3, 29–31	3.29	183	124	44	38
1H-3, 39–41	3.39	242	199	49	36
1H-3, 49–51	3.49	553	220	38	18
1H-3, 69–71	3.69	241	173	67	54
1H-3, 79–81	3.79	348	172	84	34
1H-3, 89–91	3.89	296	156	59	60
1H-3, 99–101	3.99	48	66	33	31
1H-3, 99–101	3.99	47	64	32	34
1H-3, 109–111	4.09	85	59	26	18
1H-3, 119–121	4.19	134	168	31	26
1H-3, 129–131	4.29	61	128	31	48
1H-3, 139–141	4.39	24	97	26	28
1H-3, 148–150	4.48	24	109	14	37
1H-4, 19–21	4.69	34	83	23	19
1H-4, 29–31	4.79	8	60	9	16
1H-4, 49–51	4.99	233	128	32	13
1H-4, 59–61	5.09	379	172	43	30
1H-4, 69–71	5.19	291	179	72	57
1H-4, 89–91	5.39	157	152	45	98
1H-4, 99–101	5.49	18	76	15	55
1H-4, 109–111	5.59	9	80	22	66
1H-5, 9–11	6.09	5	130	22	25
1H-5, 19–21	6.19	38	137	31	24
1H-5, 29–31	6.29	323	158	29	28
1H-5, 39–41	6.39	286	243	56	53
1H-5, 49–51	6.49	196	248	52	78
1H-5, 49–51	6.49	220	252	53	85
1H-5, 59–61	6.59	88	192	35	95
1H-5, 69–71	6.69	85	171	59	103
1H-5, 79–81	6.79	78	322	54	86
1H-5, 89–91	6.89	64	201	54	91
1H-5, 99–101	6.99	66	192	26	64
1H-5, 109–111	7.09	64	236	39	85
1H-5, 119–121	7.19	121	216	30	58
1H-5, 119–121	7.19	128	218	31	57
1H-5, 129–131	7.29	0	23	4	10
1H-5, 142–145	7.42	0	13	1	4
1H-5, 149–151	7.49	1	23	1	9
2H-1, 9–11	7.89	2	9	3	6
2H-1, 19–21	7.99	65	197	61	110
2H-1, 29–31	8.09	37	153	43	63
2H-1, 39–41	8.19	0	10	5	7
2H-1, 49–51	8.29	6	104	53	30
2H-1, 49–51	8.29	4	101	36	43
2H-1, 59–61	8.39	48	204	56	40
2H-1, 69–71	8.49	53	189	56	26
2H-1, 79–81	8.59	116	194	83	40
2H-1, 89–91	8.69	18	88	63	35
2H-1, 99–101	8.79	39	104	74	43
2H-1, 109–111	8.89	27	90	63	45
2H-1, 119–121	8.99	33	157	65	65
2H-1, 129–131	9.09	33	178	64	62
2H-1, 139–141	9.19	30	120	36	38
2H-1, 139–141	9.19	29	121	37	36
2H-1, 148–150	9.28	98	176	60	61
2H-2, 9–11	9.39	101	188	61	62
2H-2, 19–21	9.49	66	151	65	50
2H-2, 29–31	9.59	271	141	93	70
2H-2, 39–41	9.69	268	162	101	86
2H-2, 49–51	9.79	270	232	135	90
2H-2, 59–61	9.89	222	216	131	79
2H-2, 69–71	9.99	255	205	139	65
2H-2, 79–81	10.09	242	255	65	75
2H-2, 89–91	10.19	192	291	73	78
2H-2, 99–101	10.29	198	253	63	83
2H-2, 109–111	10.39	177	256	101	82
2H-2, 119–121	10.49	129	203	83	70
2H-2, 129–131	10.59	152	204	80	95
2H-2, 139–141	10.69	134	187	62	70
2H-2, 148–150	10.78	177	218	103	95
2H-3, 9–11	10.89	102	157	73	60
2H-3, 19–21	10.99	140	212	86	56
2H-3, 29–31	11.09	56	117	58	55
2H-3, 29–31	11.09	59	121	64	49
2H-3, 39–41	11.19	3	66	18	32
2H-3, 49–51	11.29	137	133	42	47
2H-3, 59–61	11.39	164	144	46	32
2H-3, 69–71	11.49	153	145	60	47
2H-3, 79–81	11.59	123	125	73	41
2H-3, 89–91	11.69	64	145	70	58
2H-3, 99–101	11.79	136	181	59	48
2H-3, 109–111	11.89	236	220	53	41
2H-3, 119–121	11.99	157	209	53	43
2H-3, 129–131	12.09	59	127	41	36
2H-3, 139–141	12.19	70	136	51	43
2H-3, 148–150	12.28	27	63	27	31
2H-4, 9–11	12.39	15	57	17	38
2H-4, 19–21	12.49	72	113	27	56
2H-4, 29–31	12.59	13	78	14	35
2H-4, 39–41	12.69	206	124	40	46
2H-4, 39–41	12.69	220	125	42	44
2H-4, 49–51	12.79	325	167	72	34
2H-4, 59–61	12.89	129	121	61	29
2H-4, 69–71	12.99	68	110	97	43
2H-4, 79–81	13.09	96	86	122	61
2H-4, 89–91	13.19	90	77	43	31
2H-4, 99–101	13.29	22	127	24	34
2H-4, 109–111	13.39	68	217	22	31
2H-4, 119–121	13.49	87	226	22	29
2H-4, 129–131	13.59	57	172	17	41
2H-4, 139–141	13.69	8	68	16	18
2H-5, 9–11	13.89	6	45	15	11
2H-5, 19–21	13.99	31	122	32	21
2H-5, 29–31	14.09	121	148	46	27
2H-5, 39–41	14.19	221	96	74	48
2H-5, 49–51	14.29	139	89	96	45
2H-5, 59–61	14.39	138	123	127	80
2H-5, 69–71	14.49	128	148	149	60
2H-5, 79–81	14.59	76	105	86	35
2H-5, 89–91	14.69	75	111	51	32
2H-5, 99–101	14.79	160	235	37	50
2H-5, 109–111	14.89	109	229	63	36
2H-5, 119–121	14.99	72	106	37	20
2H-5, 129–131	15.09	47	108	84	18
2H-5, 139–141	15.19	34	137	89	32
2H-6, 9–11	15.39	0	9	4	17
2H-6, 19–21	15.49	18	49	11	45
2H-6, 32–34	15.62	3	34	5	19
2H-6, 39–41	15.69	4	65	15	34
2H-6, 49–51	15.79	24	130	17	18
2H-6, 59–61	15.89	59	70	17	13
2H-6, 69–71	15.99	131	54	15	17
2H-6, 79–81	16.09	72	62	17	22
2H-6, 89–91	16.19	0	12	10	11
2H-6, 99–101	16.29	8	29	14	28
2H-6, 109–111	16.39	1	28	9	32
2H-6, 119–121	16.49	2	78	9	27
2H-6, 129–131	16.59	20	128	9	26
2H-6, 139–141	16.69	2	59	12	20
2H-6, 148–150	16.78	0	46	12	28
2H-7, 9–11	16.89	0	27	7	28
2H-7, 19–21	16.99	7	62	11	30
2H-7, 32–34	17.12	58	241	13	46
2H-7, 39–41	17.19	66	232	17	67
2H-7, 39–41	17.19	62	232	18	62
2H-7, 49–51	17.29	23	92	27	49
2H-7, 59–61	17.39	8	41	25	58
2H-7, 69–71	17.49	13	53	19	56

*ODP depth assignment = depth has not been adjusted.